ANALYSIS OF THE INTEGRATED AND SPECTRAL POWER EFFICIENCY OF THE AMORPHOUS PV CELL

A dissertation submitted to the University of Manchester for the degree of Master of Science in the Faculty of Engineering and Physical Science

2014

NOUF SAAD ALKATHRAN

SCHOOL OF ELECTRICAL AND ELECTRONIC ENGINEERING

Dedication

To my beloved parents,

Saad and Fawziah

Acknowledgments

It has been a privilege that Prof. Bruce Hamilton supervised by dissertation; I gratefully acknowledge his continuous support and guidance throughout. I would like to also thank Dr. Eric Whittaker for help with the experimental set up.

I deeply thank my husband, Abdullah, for his support and encouragement during the course of my study in the UK. Thanks to my children for their understanding and their endless love and patience.

Special gratitude to my beloved parents, as they have always encouraged and motivated me towards success.

Abstract

Solar photovoltaic technologies are the most affordable, obtainable, and cleanest of energy resources that are attracting the worldwide interest of energy communities, engineers, and researchers. Research is focused in examining and analysing the efficiency of photovoltaic novel cells in order to investigate the potential area for boosting their performance.

This work examines the efficiency of an amorphous silicon solar cell sample with an illuminated area of 35 mm^2 in comparison to a standard crystalline silicon solar cell with an illuminated area of 1.77 mm^2, using a solar simulator. Current-voltage measurements show that the integrated amorphous silicon solar cell recorded an efficiency of 0.293% and the integrated crystalline silicon solar cell reported an efficiency of 5.210%. The efficiency of both solar cells was analysed with respect to centre wavelengths of the transmission curve of five filters; FB390, FB470, FL514.5, FB730, and FB880-40, in order to identify the spectral power efficiency of both solar cells. The fitted curve of the spectral power efficiency of both solar cells indicates that short wavelengths up to 465 nm could be converted more efficiently by the amorphous silicon solar cell than the crystalline silicon solar cell due to the high-energy gap of the former semiconductor. However, at the visible and near infrared light regions, the efficiency of the crystalline silicon solar cell outweighs the amorphous silicon solar cell. It seems that recombination mechanisms are the dominant reason for reduced efficiency of the amorphous silicon solar cell in the visible light region from 465-750 nm. Long wavelengths greater than 750 nm are most likely to be dissipated since their energy is lower than the energy gap of the amorphous silicon solar cell, which in turn causes efficiency degradation.

Table of Contents

(Words: 22,984)

List of Figures

List of Tables

1 Introduction

1.1 Motivation

An increase in energy demand due to economic and world population growth has led to a significant increase in fossil fuel consumption. Fossil fuels such as oil, gas and coal are the primary energy supplies in the present energy scenario. Combustion of such fuels omits carbon dioxide emissions into the atmosphere. This in turn is a major cause of climate change (Rhys, 2011). However, an increase in worldwide awareness of global warming and increased oil prices have both led to a change in some of the energy policies to be more environmentally friendly. Utilisation of renewable sources will help to protect the environment and to provide energy security. A major drive towards renewable energy development was provided by the Kyoto protocol (1998). This was an attempt to bind the international action on greenhouse emissions. Developed countries have already responded to the international commitment to limit their emissions by increasing the energy production from clean energy sources. Consequently, the Renewable Energy Directive (2008) was adopted by the European Union, which aims to produce 20% of the total energy consumption from renewable sources by 2020.

Solar energy is the most obtainable, inexhaustible and promising source of renewable energy sources. Solar energy can be utilized in two techniques. Firstly, it can be used directly to provide heat or to operate steam turbines as in concentrating solar power (CSP). Secondly, solar radiation can be used to generate electricity by photovoltaic technologies (PV). PV electricity production has been rapidly developed as a result of PV technology development and government incentives. At present, worldwide PV electricity production has reached about 23.5 GW (Tyagi *et al.*, 2013).

Historically, single crystalline silicon semiconductors material attracted researchers' interest the most. In the 1950s, the efficiency of the single crystalline silicon solar cell was only 15% and then improved to 17% in the 1970s. Nowadays, it achieves up to 28% efficiency (Tyagi *et al.*, 2013). In spite of the advance development in the efficiency of crystalline silicon solar cells, the cost of manufacturing processes is still an obstacle. The high cost associated with the production of crystalline solar cells contrasts with the aim of PV research, which aims to produce efficient and cheap solar cells. The production of crystalline silicon solar cells consumes too much material, which leads to waste silicon material. In addition, the manufacturing conditions of high temperature and operating under a vacuum contribute to higher cost. Further, these conditions consume significant amounts of energy leading to increased carbon dioxide levels in the atmosphere (Vetterl *et al.*, 2000). As a consequence, research interest has shifted towards alternative materials. Amorphous silicon semiconductors have become a promise alternative due its' optical absorption properties, which will be discussed later (section 2.4.2). The interest in

amorphous silicon solar cells has increased since they can be made as thin films; hence their productions consume lower silicon material comparing to crystalline silicon solar cells. Moreover, the manufacture processes of amorphous silicon solar cells do not require high temperatures, which gives flexibility in the use of low cost substrate materials such as glass and plastic (Wagner *et al.,* 1999; Vetterl *et al.*, 2000).

1.2 Research Objectives

Continued effort and research to investigate the performance of amorphous silicon solar cells are essential to understand their efficiency limitation factors. This is because the physics of amorphous silicon solar cells is not fully understood yet (Gottschalg *et al.,* 2005). This dissertation aims to measure the power conversion efficiency of both a standard crystalline solar cell and an amorphous silicon solar cell under the integrated extraterrestrial solar spectrum (AM0) by using a solar simulator. The efficiency measurement will be identified at particular wavelengths (390, 470, 514.5, 730, and 880 nm) to determine the spectral power efficiency of both types of silicon solar cells. The objectives of this dissertation are:

- Conduct research about the performance indicators of solar cells and factors that limit their efficiency.
- Conduct current-voltage measurements under the entire solar spectrum AM0 for a standard crystalline silicon solar and an amorphous silicon solar cell.
- Conduct current-voltage measurements for both solar cells under particular wavelength bands of the solar spectrum by adjusting different filters on the top of each solar cell.
- Plot current-voltage curves for all measurements and estimate the maximum output power of both solar cells illuminated under particular wavelength bands.
- Estimate the total input power of the solar radiation through each filter, and then calculate the power conversion efficiency of both solar cells.
- Plot the power conversion efficiency resulting from different wavelength bands with respect to the central wavelength of each filter for both solar cells to identify the spectral power efficiency of both solar cells.
- Compare the spectral power efficiency of both the crystalline silicon and amorphous silicon solar cells and identify the possible reasons for different findings, and therefore, write appropriate conclusions.

1.3 Dissertation Overview

This dissertation comprises seven chapters starting with this introductory chapter and ending with conclusions. The remaining of this chapter details the general underlying principles of the solar cell and the p-n junction. In the second chapter, the theoretical background of solar cells is reviewed. This includes the essential operation processes and common performance indicators of

solar cells, along with the important reasons for power conversion efficiency degradation that influence the effectiveness of solar cells. The concept behind the amorphous silicon solar cell and its potential is discussed and a literature review of amorphous silicon performance is cited. Thereafter, the experimental set up adopted to achieve the aim of this dissertation and the experiment analysis are addressed in the methodology and analysis chapters, respectively. Finally, the findings of the dissertation are presented in the conclusions and future work chapter.

1.4 Solar Cell

A solar cell is a term describing a system, which converts light into electricity (Fonash, 2010). A solar cell is made of semiconductor materials. Semiconductor atoms connect to each other by covalent bonds, where each atom shares an electron to form the bond. Semiconductors can consist of a single element such as Si and Ge or two elements such as GaAs or CdTe. Usually, at very low temperature (zero Kelvin) semiconductors work as insulators. This is because electrons do not have enough energy to break these strong covalent bonds. Consequently, the electrons locate in the valence band as they cannot cross the band gap to the conduction band where they can contribute to conductivity. The band gap is a gap that separates the valence band and the conduction band, and its energy is dependent on the materials of the semiconductor (PV EDUCATION.ORG).

The practical method to enhance the conductivity of semiconductors is doping. The doping mechanism can make a pure semiconductor either p-type or n-type. The former is obtained when doping enhances the number of 'holes'. A hole is a charge carrier that equals to the electron charge but with a positive charge. This could be obtained by doping the semiconductor with an element that has three valence electrons, usually boron. In contrast, the latter, i.e., n-type semiconductors, are obtained when the doping increases the number of electrons. Five-valued elements, usually phosphorus, are used to produce n-type semiconductors (PV EDUCATION.ORG).

The most common form of solar cells is the p-n junction (Nelson, 2003). This form is prepared by putting p-type and n-type semiconductors in contact. As a consequence, some free electrons transmit from the n- to p-type causing positive charges in the n-type beside the junction. At the same time, some free holes transmit from the p- to n-type creating negative charges in the p-type beside the junction. The positive and negative charges create an electric field (E), which in turn prevents the diffusion of additional free electrons and holes. Hence, a depletion region is created at the p-n junction (Willis, 2011). The existence of the electric field leads to built-in voltage (V_{in}). The electric field created at the p-n junction and the built in voltage are shown in Figure 1 (Willis, 2011). The electric field acts as a diode since it controls the direction of electrons; electrons flow only from p- to n-type and holes flow from n- to p-type. When photons with enough energy (equals or greater than the energy gap of the solar cell) fall on the solar cell, they are absorbed

near the depletion region resulting in a free electron-hole pair (minority carriers) (Willis, 2011; Kitai, 2011).

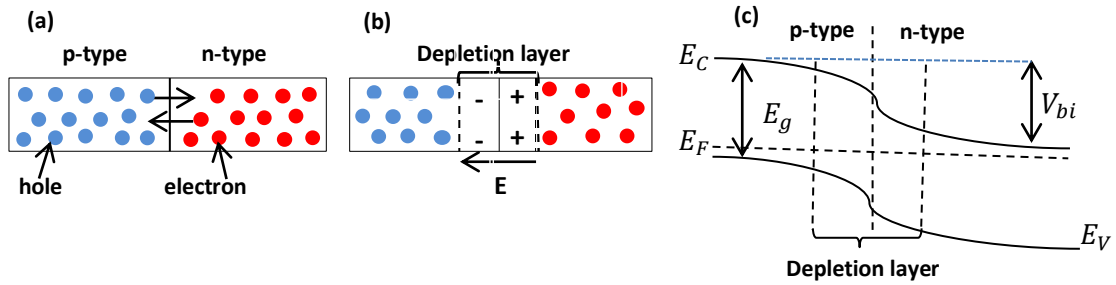

Figure 1: Structure of a p-n junction.

(a) Electrons in n-type and holes in p-type flow in reverse direction. (b) Depletion layer is existed beside the p-n junction containing positive and negative ions which create an electric field, E. (c) Energy level structure of p-n junction at equilibrium, the voltage built in (V_{bi}) is equivalent to the energy gradient.

2 Theoretical Background

2.1 Solar Cell Operation

Although there are different types of solar cell technologies, generating electrical power is based on the same principal. This principal includes three essential steps; light absorption, minority carriers separation, and minority carriers extraction (Haberlin, 2012; Julian Chen, 2011; Willis, 2011). Firstly, incident light is absorbed by a solar cell resulting in generation of free electron-hole pairs in the solar cell. When the energy of incident photons $(\frac{hc}{\lambda})$ is equal to or greater than the energy gap of a solar cell, an electron can be excited to the conduction band causing a positive charge (hole) in the valence band; otherwise, the energy of these photons will be lost. Both the electron and hole contribute to generate electrical power. This process is known as light absorption. Secondly, the electric field at the p-n junction is an important factor, which separates the minority carriers; otherwise, these carriers will recombine. The time required in order to separate generated electrons and holes depends on the width of the depilation region (Zamen, 2006). The electric field will direct the generated minority carriers: electrons to the n-type and the holes to the p-type. The depletion region then collects these minority carriers to produce photocurrent. The final step is extracting the generated carriers from the depletion region by a metal electrode on either the front or the back surface of solar cells (Haberlin, 2012; Julian Chen, 2011; Willis, 2011).

2.2 Performance Indicators of Solar Cells

The main indicator to assess the performance of solar cells is the maximum output power that can be generated from solar cells. This is because the price of solar systems primarily depends on the amount of useful power generated (Tyagi *et al.,* 2013). A range of different strategies can be followed to obtain the parameters of solar cells; hence, solar cells can be assessed (Nann and Emery, 1992).

2.2.1 Current *versus* Voltage Measurements

Current *versus* voltage measurements are the most fundamental measurement used to characterize and evaluate the effectiveness of solar cells in converting light into electricity. Operating a solar cell under a light source leads to draw photocurrent. The current-voltage measurement of a test cell, illuminated by a light source, is completed by measuring the irradiation density of the light source followed by measuring the generated voltage and current at different levels of external power supply. The photocurrent and the bias voltage across the test cell are recorded by current/voltage ammeter. Hence, an I-V curve can be plotted in the fourth quadrant. Analysing this curve of any solar cell gives the essential performance parameters: the short circuit current(I_{SC}), the open circuit voltage (V_{OC}), and the maximum output power (P_{Max})

(Emery, 2003). The short circuit current is the maximum current produced from a solar cell at zero bias voltage. The short circuit current usually reduces due to optical losses because the incident light that can be absorbed to generate current is limited. The open circuit voltage is the maximum voltage created across a solar cell when the forward current cancels out the reverse current. The open circuit voltage significantly reduces due to recombination mechanisms. The maximum electrical power produced from solar cells is indicated as the knee point of the I-V curve. It depends on both short circuit current and open circuit voltage. Figure 2 shows the characteristics of the I-V curve including the estimated maximum power point (Hernday, 2011). The maximum output power is calculated by multiplying the maximum generated current (I_{mp}) by the maximum voltage(V_{mp}). The maximum current and voltage are obtained by drawing two lines from the maximum power point to the y- and x-axis (see Figure 2).

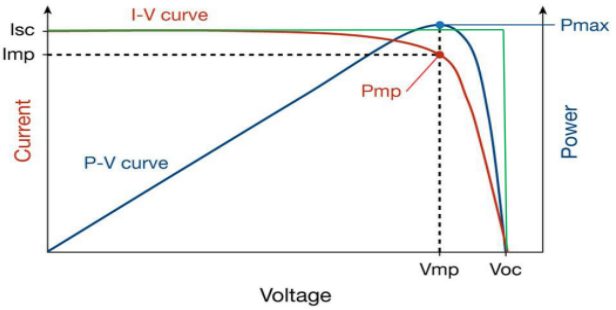

Figure 2: Typical I-V curve characteristic of solar cells.
The red curve presents the measured photocurrent with respect to voltage bias. The short circuit current, I_{SC} is maximum generated current at zero voltage bias whereas the current collapse to zero at open circuit voltage, V_{OC}. The area under rectangular black dash gives the maximum power output. The blue curve shows the generated power with respect the bias voltage (Hernday, 2011).

2.2.1.1 Fill Factor

The fill factor (FF) is an important parameter, which describes the quality of solar cells. It measures the ratio of the maximum generated power (P_{Max}) to the optimum power that can be produced from the solar cell at the short circuit current and open circuit voltage. Hence, according to the I-V curve (Figure 2) the fill factor is given as the area of the large rectangle (green) over the small rectangle (black dashed line). High fill factor values indicate how efficient solar cells are. The following equation can be used to estimate the fill factor value (Haberlin, 2012; Tao, 2014; KEITHELY Instrument Aapplication Note Series, 2000):

$$FF = \frac{P_{Max}}{P_{opt}} = \frac{I_{mp}V_{mp}}{I_{SC}\,V_{OC}} \qquad \text{Eq. (1)}$$

Hence, the optimum value of the fill factor is equal to one. However, solar cells may not always achieve the theoretically optimum fill factor. This could be due to series resistance, electron-hole recombination, and other factors, which will be discussed later (section 2.3). As a result of series

resistance (R_S), the fill factor predicted from an ideal cell (FF_0) reduces to the (FF). The fill factor of solar cells is given by (Zhou *et al.,* 2007; Markvart and Castañer, 2012):

$$FF = FF_0(1 - r_s) \qquad \text{Eq. (2)} \qquad \text{while } r_s = R_S \frac{I_{SC}}{V_{OC}} \qquad \text{Eq. (3)}$$

2.2.1.2 Efficiency

The power conversion efficiency (η) is the most common indicator used to describe the performance of solar cells. The efficiency indicator determines the ability of a solar cell in converting the incident light energy on its surface into electrical power. Hence, the efficiency of solar cells can be written as the maximum generated power (P_{Max}) divided by the input power of the incident light (E_{tot}) on the surface area (A) of the solar cell (Julian Chen, 2011; Emery and Moriarty, 2008; Emery, 2003):

$$\eta = \frac{P_{Max}}{E_{tot}\, A} \qquad \text{Eq. (4)}$$

The efficiency of solar cells varies from zero to one. The variation in the solar cell efficiency depends on the produced value of the fill factor, the short circuit current, and the opens circuit voltage as described in the following equation (Haberlin, 2012; Tao, 2014):

$$\eta = \frac{FF\, I_{SC} V_{OC}}{E_{tot}\, A} \qquad \text{Eq. (5)}$$

Practically, solar cell efficiency is limited owing to many loss mechanisms due to light losses, carriers' behaviour, or both. Different reasons behind limiting the efficiency of solar cells are discussed in section 2.3.

2.2.2 Quantum Efficiency and Spectral Response

Quantum efficiency measurements can also be used to identify losses, which lead to efficiency degradation. Quantum efficiency $QE(\lambda)$ gives information about the number of generated charge carriers to the number of photons in the incident light at a specific wavelength in the unit of electron per photon. Simply put, it measures how the electrical properties of the solar cell respond to light at different wavelengths. The $QE(\lambda)$ of solar cells that identifies information about the generation and losses is known as the external quantum efficiency $EQE(\lambda)$, as it considers all photons in the incident light including photon losses. However, another term of $QE(\lambda)$ is the internal quantum efficiency, $IQE(\lambda)$; it takes into consideration only photons that contribute to carriers' generation, excluding losses resulting from optical losses or reflection losses. Hence, the IQE value is normally close to one while the EQE is much lower (Markvar and Castañer, 2012; Nagle, 2007). $QE(\lambda)$ measurements are normally carried out at different wavelengths ranging from ultraviolet to infrared; this is to identify the quantum efficiency of solar cells over different energy levels of the solar spectrum. The percentage of QE is plotted as a

function of photon wavelength(λ). The $QE(\lambda)$ curve of a measured crystalline silicon solar cell and an ideal crystalline silicon solar cell are shown in Figure 3a (PV EDUCATION.ORG). It can be observed that the $QE(\lambda)$ curve of an ideal solar cell has approximately a square shape, where its end at the cut-off wavelength $\left(\frac{1240}{E_g(eV)}\right)nm$ depends on the energy gap of the solar cell (Photodiode Technical information). Interestingly, the $QE(\lambda)$ curves of both a measured and an ideal crystalline silicon solar cell cover the same area from 0-1100 nm. This is because the power conversion of the crystalline silicon solar cell is limited up to 1100 nm since the energy gap of crystalline silicon is approximately 1.12 eV. However, the $QE(\lambda)$ curve of the measured cell is lower than the theoretical value of the ideal solar cell. At short wavelengths region, light has high energy; hence, it is absorbed at the solar cell surface. Light absorption at this level is often affected by the surface recombination mechanism. Additionally, the extra energy of absorbed photons is lost as heat. Together, these mechanisms decrease the $QE(\lambda)$ of solar cells. The $QE(\lambda)$ of the measured cell in the visible light region reduces as a result of photon losses due to light reflection at the solar cell surface. Whereas in the long wavelength region, the $QE(\lambda)$ usually reduces due to transmission losses or due to recombination losses at the rear surface of the solar cell (Strümpel, 2007).

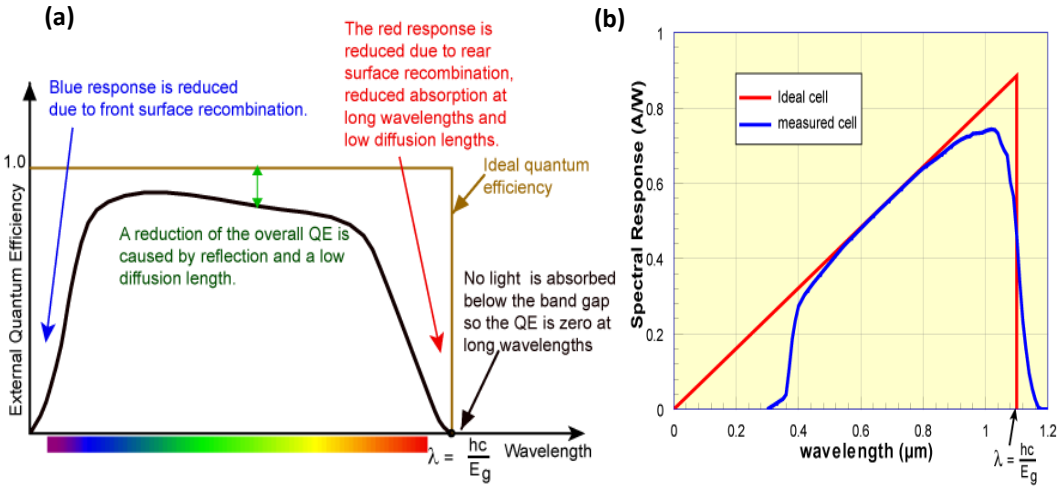

Figure 3: (a) External quantum efficiency and (b) Spectral response with respect to photon wavelengths of an ideal solar cell and a measured solar cell.
Both curves end at a photon energy equal to the energy gap of the solar cell. Measured solar cell performance shows a reduction especially at short and long wavelengths (PV EDUCATION.ORG).

The spectral response $S(\lambda)$ of solar cells gives similar meaning to the quantum efficiency $QE(\lambda)$. The difference is that the former measures the produced photocurrent with respect to the spectral irradiance at a particular wavelength. Hence, the unit of the spectral response is ampere per watt in contrast with that of the quantum efficiency, which is expressed as electron per photon. The spectral response as a function of wavelength of an ideal crystalline silicon solar cell and a measured crystalline silicon cell is shown in Figure 3b. The curve of a measured solar cell

deviates from that of an ideal solar cell due to the same reasons that reduce the quantum efficiency of a measured cell. Different measurement systems have been developed to evaluate the spectral response of solar cells such as grating-monochrometer and interference filters (Emery, 2003; Markvar and Castañer, 2012). At a given quantum efficiency at a particular wavelength, the spectral response of solar cells can be calculated as (Castañer and Silvestre, 2002):

$$S(\lambda) = \frac{q}{hc}\,\lambda\,QE(\lambda) \qquad \text{Eq. (6)}$$

where h is the Planck constant, q is the electron charge, c is the light speed.

2.3 Loss Mechanisms in Solar Cells

The energy gap of solar cells plays a key role in determining the efficiency of solar cells. Previously, it was observed that an increase in efficiency is associated with the increase of the output power determined by the photocurrent times the bias voltage. A large band gap results in a large open circuit voltage, while a small band gap leads to large photocurrent (Wilis, 2011). This means that there is an optimum band gap that gives an optimum efficiency. It is found that the optimum energy gap of semiconductors materials under the solar spectrum AM0 is approximately 1.3 eV and this can achieve an efficiency of about 31% (Araujo and Marti, 1994). Figure 4 displays the optimum efficiency of a single junction wafer-Si, CdTe, amorphous-Si, and CIGS solar cells with respect to the energy gap under the solar spectrum AM 1.5. However, the efficiency of these solar cells does not reach the optimum values. For example, the maximum efficiency of a single junction wafer silicon cell is above 33% while the actual efficiency that has been reached is only 25% (Tao, 2014).

Indeed, there are several factors limiting the efficiency of solar cells. These factors could be classified under loss mechanisms as optical, recombination and resistive losses. Reducing these loss mechanisms at the lowest cost is an essential solution to improve the efficiency of solar cells (Julian Chen, 2011; Haberlin, 2012; Tao, 2014).

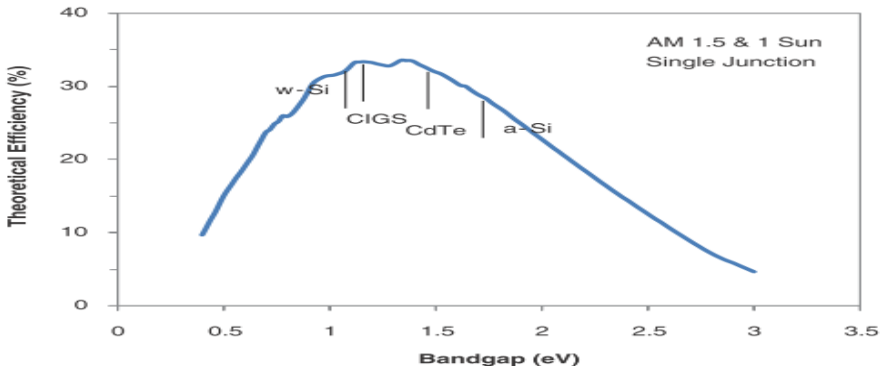

Figure 4: Theoretical efficiency with respect to band gap of different solar cells (Tao, 2014).

2.3.1 Optical losses

Optical losses can occur due to weak or excessive energy of incident photons, light reflection at solar cell surfaces, incomplete absorption of incident light in the absorber layer and shadowing loss of a top metal contact (Prajapati, 2013; Tao, 2014). Solar irradiation comprises a wide range of electromagnetic waves of different wavelengths (λ), which have different energy levels (E). Some photons do not have an adequate energy to boost electrons to the conduction band. This is because their energy is lower than the energy gap (E_g) of a solar cell. Consequently, the energy of these photons is dissipated since they cannot be converted to electrical power (Solanki, 2009). They pass through the solar cell without inducing any significant effect. However, there are some photons that have energies greater than the energy gap of a solar cell; hence, these photons are absorbed and their extra energy is lost in the form of thermal energy (Solanki, 2009). Trupke *et al.* (2002) suggest a down-conversion method for classical single junction solar cells to solve the thermal loss owing to absorption of high-energy photons. The use of luminescence converter on the top surface of solar cells converts any photon which has energy greater than twice the energy gap into two photons with lower energy. Down-conversion strategy has successfully recorded an efficiency improvement of about 9%. Another solution to reduce the optical losses due to low and high-energy photons is manufacturing solar cells with multi-junctions, such as Tandem solar cells. These types of solar cells are made of different materials with a different energy gap in order to match the solar spectrum (Julian Chen, 2011; Haberlin, 2012; Tao, 2014).

Another form of optical losses is the reflection loss from the front surface of solar cells. When light transfers between two materials with different refractive indices, for example, light travel from air to a solar cell, part of incident light does not enter the solar cell since it reflects from the solar cell surface. The reflectance (r) between air and a solar cell material is calculated by the Fresnel equation:

$$r = \left|\frac{n_0 - n_{sc}}{n_0 + n_{sc}}\right|^2 \qquad \text{Eq. (7)}$$

where n_0 is the refractive index of air and n_{sc} is the refractive index of solar cell material (Prajapati, 2013).

Typically, anti-reflection coating techniques are adopted to manage the reflection loss. This technique is carried out by applying a thin transparent film of a thickness, d, and a refractive index, n_{ar}, between the glass or ethylene vinyl acetate (EVA) and the absorber material. The total reflection (R) is then calculated by (Tao, 2014):

$$R = \frac{r_0^2 + r_{sc}^2 + 2r_0 r_{sc}\, cos2\beta}{1 + r_0^2 r_{sc}^2 + 2r_0 r_{sc} \cos 2\beta} \qquad \text{Eq. (8)}$$

where $r_0 = \frac{n_{ar} - n_0}{n_{ar} + n_0}$, $r_{sc} = \frac{n_{sc} - n_{ar}}{n_{sc} + n_{ar}}$, $\beta = \frac{2\pi}{\lambda}\, n_{ar}\, d$

Hence, the transmission coefficient (T) is given by (Tao, 2014):

$$T = 1 - R \qquad \text{Eq. (9)}$$

To limit the reflection, the quarter wavelength condition is adopted to determine the best characteristics of the anti-reflection layer. The optimum thickness (d) and refractive index (n_{ar}) values of the anti-reflection layer are given by (Julian Chen, 2011; Haberlin, 2012; Prajapati, 2013; Tao, 2014) :

$$d = \frac{\lambda}{4\, n_{ar}} \qquad \text{Eq. (10)} \qquad\qquad n_{ar} = \sqrt{n_0\, n_{sc}} \qquad \text{Eq. (11)}$$

The effectiveness of an anti-reflection layer works for a particular wavelength at a particular incident angle. Since the solar spectrum consists of a wide range of wavelengths with a different incident angle throughout the day and year, another technique, besides the anti-reflection layer, should be used. Surface roughening techniques are used to trap sunlight in order to increase the probability of light absorption. The pyramidal texturing method is a good example of such a technique, which minimises light reflection (Carson, 2008). The combination of anti-reflection and roughening techniques can limit light reflection loss; hence, the solar cell performance improves. It should be noted that the pyramidal texturing technique works effectively only on mono-crystalline silicon; it is not efficient on other solar cells such as multi-crystalline silicon and amorphous silicon. This is because the anisotropic nature of mono-crystalline silicon fits a pyramidal surface texture. However, there are many roughening techniques have been developed for multi-crystalline and amorphous silicon cells (Tao, 2014).

Shadowing loss is another form of optical losses caused by metal electrode coverage. The front metal electrode reduces the transparent area of the solar cell surface. This reduces the amount of incident photons entering solar cells, thus reduces the generation of minority carriers, which leads to decreased output power. The active transparent area of solar cells surface is defined by a coverage factor (Tao, 2014), which is given as the ratio of the transparent area that is not covered by metal (A_f) to the total area of the solar cell surface (A_{tot}). To minimise shadowing loss, the

coverage factor should be as high as possible. This can be achieved by designing the front electrode in a 'finger shape' with small width and high height. The reduction in the metal fingers width leads to an increase in the series resistance loss. Hence, a high coverage factor and low series resistance should be taken into account when designing metal fingers. Therefore, an optimum grid pattern is designed to minimise both losses of shadowing and series resistance of the metal front contact (Ludowise and Frass, 2010). In addition, the use of the metal electrode on the back surface of solar cells could avoid the issue of shadowing loss. Back contact solar cells have shown an efficiency improvement; for example, commercial solar cells with the back contact surface have recorded an efficiency of 24.2% (Tao, 2014).

Optical loss could be owing to incomplete absorption of incident light, which is determined by the absorption coefficient (α). Since the thickness of the absorber layer of solar cells is finite, some incident light may leak from the front or the back surfaces of solar cells (Solanki, 2009). Consequently, some photons escape from solar cells without converting; hence, the power conversion efficiency of solar cells reduces. Such optical loss is significant for indirect band gap semiconductors such as crystalline silicon (c-Si). The indirect band gap leads to a long extinction depth (1/α). In other words, indirect band gap leads to small absorption coefficients. To ensure that light is perfectly absorbed, light should be trapped inside the solar cell. This means that the front and the back surfaces of solar cell should act as reflectors. A back metal reflector is designed to return photons into the absorption layer again (Haberlin, 2012; Tao, 2014). However, a metal reflector is not a good choice for the front surface as it prevents light from entering solar cells. Incident light is reflected from the back surface to the front surface of solar cells. At the front surface, the backward light (the reflected light) is exposed to the total internal reflection because the backward light (the reflected light) travels from a high refractive index of the solar cell to a low refractive index of the anti-reflection coat. The total internal reflection of the backward light occurs at a critical incident angle. Beyond the critical angle, the backward light is exposed to specular reflection; hence, the backward light returns into the solar cell. However, if the incident angle of the backward light is smaller than the critical value, the backward light leaks from the front surface (Würfel, 2009; Tao, 2014).

Figure 5 shows some of the optical losses discussed previously in a wafer silicon solar cell. It represents optical losses due to shadowing, reflection and incomplete light absorption.

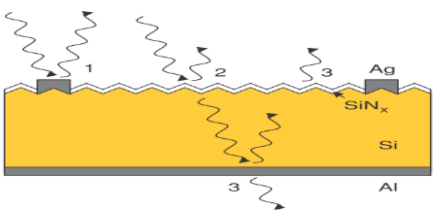

Figure 5: Optical losses in a wafer silicon solar cell with an aluminium back surface reflector.
1) Shadowing loss due to metal electrode. 2) Reflection loss at front surfaces. 3) Leaking loss from both front and back surfaces (Tao, 2014).

2.3.2 Recombination losses

Light absorption by solar cells leads to excitation of electrons to the conduction band and creates positive charges (holes) in the valence band. Electron-hole pairs are then collected by a metal electrode and extracted through an external load. Generated electron-hole pairs can recombine before reaching the electrode, which in turn results in lowering the power conversion efficiency of solar cells. Naturally, free charge carriers tend to recombine to reach a stable condition. The recombination mechanism due to carriers' behaviour is considered as the main reason for degrading the efficiency of solar cells. Additionally, the recombination mechanism is an important factor in determining the lifetime of free charge carriers. Electron-hole recombination might exist in the bulk of solar cells through three pathways: band-to-band recombination, recombination through defects, and Agure recombination (Rein, 2006). Figure 6 shows the differences between these types of recombination mechanisms (Tao, 2014).

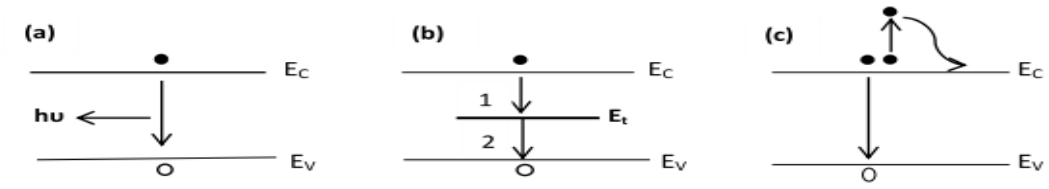

Figure 6: Three types of bulk recombination mechanisms in solar cells.
(a) Band-to-band recombination results in photon emission with energy = hu. (b) Recombination through deep level states in the mid-gap, where an electron falls into a hole in the valence band in two steps without the release of a photon. (c) Auger recombination, where an electron falls in the valence band and excites another electron to a higher level in the conduction band (Tao, 2014).

Band-to-band recombination usually occurs in direct band gap solar cells such as amorphous silicon (a-si) and GaAs. The excited electrons in the conduction band directly recombine with holes in the valence band. Direct recombination results in emitting a photon with an energy equivalent to the energy gap of the solar cell, see Figure 6a. Hence, this type of recombination is known as a radiative recombination (Sheng, 2007). The minority carriers of direct band gap solar cells conserve the momentum (K-value) of the system. This means that for the band-to-band recombination, the momentum of electrons in the conduction band and holes in the valence band must be identical. This is not the case in indirect band gap solar cells such as crystalline silicon, where the maximum energy level of the valence band and the minimum energy level of the conduction band have different momentum. Therefore, a phonon contribution is necessitated for momentum conservation. After that, electrons could recombine with holes in the valence band causing photons emission. Thus, the probability of the band-to band-recombination in indirect band gap solar cells is limited. Figure 7 shows the band-to-band recombination mechanism in direct and indirect band gap solar cells (Sun, 2010).

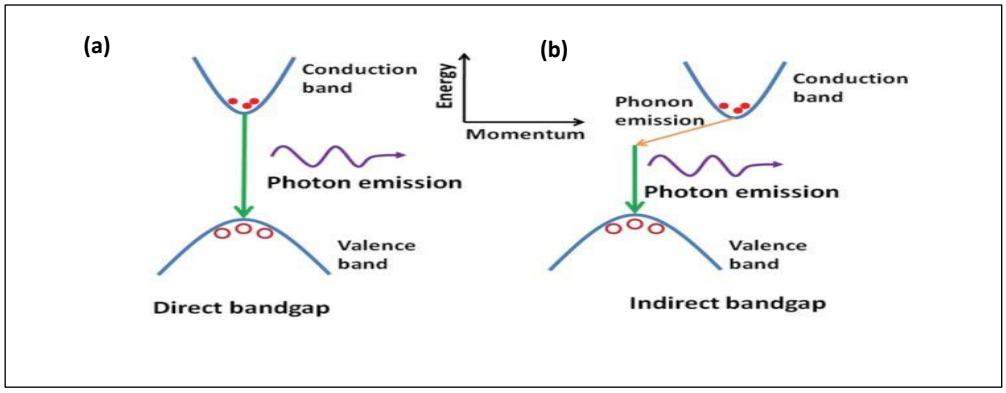

Figure 7: Band-to-band recombination processes in (a) direct and (b) indirect band gap solar cells. (a) Direct band gap solar cells release a photon when an electron falls in the valence band and the electron hole recombination is completed in one step. (b) In an indirect band gap solar cell an electron recombines with a hole in two steps and releases a phonon to maintain momentum conservation (Sun, 2010).

The recombination mechanism has impacts on the lifetime of generated electrons and holes. The carriers' lifetime is the time period since their generation until their recombination. The lifetime of generated electrons and holes in indirect solar cells, such as in wafer silicon, is about several milliseconds. This is a long period comparing to those in direct gap solar cells, which are in the range of nanoseconds (Tao, 2014; Bhattacharya, 2013). The radiative recombination lifetime (τ_r) can be estimated using the following equation (Rahman, 2012) :

$$\tau_r = \frac{1}{B(p_0+n_0)+B\Delta n} \qquad \text{Eq. (12)}$$

where B is the coefficient of radiative recombination, p_0 and n_0 are the density of holes and electrons, respectively, and Δn is the non-equilibrium electron density.

Recombination also occurs as a result of defect states in the band gap. Defect (or trap) states are energy levels with density N_T that might exist near the middle of the band gap. These energy levels increase the probability of electron-hole recombination. Recombination through the defect states is also known as Shockley-Read-Hall (SRH) recombination. It is more common in indirect gap solar cells such as crystalline silicon. This kind of recombination is introduced in two steps without photon radiation. Firstly, the generated electron falls into the deep energy level (mid gap). Thereafter, it falls further into the valence band where it recombines with a free hole (see Figure 6b). During these steps, the electron loses its energy in the form of heat and there is no requirement for a phonon as its momentum is conserved (Sheng, 2007). Such deep energy levels are created as a result of impurities or imperfections in crystal semiconductors. Metal contaminations such as iron or copper that are used in manufacturing processes are another reason for creating deep energy levels. The lifetime of non-radiative recombination in p- and n-type silicon solar cells are given by equation (13) and (14), respectively (Rahman, 2012):

$$\tau_{nr} = \frac{1}{N_t\sigma_n v_{th}} \qquad \text{Eq. (13)} \qquad \tau_{nr} = \frac{1}{N_t\sigma_p v_{th}} \qquad \text{Eq. (14)}$$

where N_t is the density of the recombination through defects, σ_n and σ_p are the capture cross section of minority carriers and v_{th} is the thermal velocity of charge carriers.

These equations show the relation of the large cross section of the minority carriers due to high doping in lowering the minority carriers' lifetime; hence, the minority carriers recombine quickly. This has a significant negative impact on the generated electrical power as the number of minority carriers that can reach the electrode decreases (Tao, 2014; Rahman, 2012).

Another type of recombination mechanism is Auger recombination. This occurs when three particles are affected by a recombination mechanism. When an electron in the conduction band directly recombines with a hole in the valence band, the extra energy of the recombined electron excites another electron in the conduction band to a higher energy level. Thereafter, the excited electron starts to lose the extra energy in a series of steps until it relaxes at the conduction band edge as shown in Figure 6c. Likewise, the extra energy of the recombined electron can be transferred to a hole in the valence band (Rahman, 2012; Bhattacharya, 2013).

The Auger lifetime in n-type solar cells for both low and high doping level are given respectively by the following equations (Altermatt *et al.,* 1997; Rein, 2006):

$$\tau_{ld} = \frac{1}{C_p N_D^2} \quad , \tau_{hd} = \frac{1}{(C_n + C_p)\Delta p^2} \qquad \text{Eq. (15)}$$

The Auger lifetime in p-type solar cells for both low and high doping level are given respectively by the following equations:

$$\tau_{ld} = \frac{1}{C_p N_A^2}, \quad , \tau_{hd} = \frac{1}{(C_n + C_p)\Delta n^2} \qquad \text{Eq. (16)}$$

where C_p and C_n are the Auger coefficients and N_D and N_A are dopant densities.

From previous equations it is clear that the Auger recombination in solar cells is heavily dependent on the high concentration of carriers (Rahman, 2012; Tao, 2014).

Recombination commonly occurs at the front and the back surfaces of solar cells. This is because atoms on the solar cell surface have dangling bonds, which creates defect states; thus, enhancing surface recombination. The surface recombination velocity (S) influences the lifetime of minority carriers (τ_s). Hence, the lifetime of minority carriers can be given by the Equation 17 (García-Tabarés and Rey-Stolle, 2014; Grivickas and Noreika, 1989 cited in Rahman, 2012):

$$\tau_{surfac} = \left(\frac{2S}{W} + \frac{1}{D_n}\left(\frac{W}{\pi}\right)^2\right)^{-1} \qquad \text{Eq. (17)}$$

where W is wafer thickness and D is the diffusion coefficient.

Surface recombination can be mitigated when the dangling bonds are treated. This can be achieved by a surface passivation method. Dielectric coating is an effective way, which works probably for both n- and p-type silicon solar cells to reduce the defect states. For example, Si wafer is coated with silicon dioxide (SiO_2). Another coating material that is used for commercial n-type Si wafer is hydrogenated SiN_X which works also as an anti-reflection surface (Tao, 2014).

Considering all recombination mechanisms, including bulk and surface recombinations, the effective carriers' lifetime can be defined as (Altermatt, 1997; Rein, 2006; Rahman, 2012):

$$\frac{1}{\tau_{eff}} = \frac{1}{\tau_r} + \frac{1}{\tau_{nr}} + \frac{1}{\tau_{Ag}} + \frac{1}{\tau_{surface}} \qquad \text{Eq. (18)}$$

2.3.3 Resistive losses

The generated electrical power may be limited due to resistances associated with the solar cell structure. Series resistance (R_S) and shunt resistance (R_{SH}) are two types of resistances, which contribute in determining the output power of solar cells. Figure 8 shows the typical circuit of solar cells, where the series resistance sets are in series with the diode and the shunt resistance sets are in parallel. The total current density drawn from such a circuit is given as (Haberlin, 2012; Tao, 2014; FÖll, 2011; Markvart and Castañer, 2012):

$$J = J_0(\exp(\frac{q(V+IR_S)}{k\,T}) - 1) + \frac{V-IR_S}{R_{SH}} - I_{Ph} \qquad \text{Eq. (19)}$$

where J_0 is the saturation current density, k is the Boltzmann constant, T is the temperature in Kelvin and J_{Ph} is the photocurrent density.

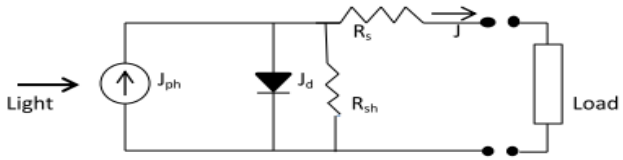

Figure 8: A typical equivalent circuit of non-ideal solar cells displaying series resistance and shunt resistance (Markvart and Castañer, 2012).

Rear contact resistance, base resistance, emitter resistance, finger and busbar resistances and the front contact resistance are different causes of series resistance in solar cells. When the generated electrons are on their way to the electrode where they can be collected, some power dissipates in the form of heat in these resistances. Generally, the resistance is given by (Tao, 2014):

$$R = \frac{\rho l}{A} \qquad \text{Eq. (20)}$$

where ρ is the resistivity, l is the length and A is the cross-section area.

Theoretically, generated electrons travel perpendicularly in the solar cell base; however, in the emitter they travel in a parallel direction with the emitter. Therefore, the resistance of the base and rear is less problematic than other resistances since their cross section areas are large. Consequently, the resistance associated with the emitter, front contact, fingers and busbar are usually used to determine the resistive losses due to the series resistance.

Resistive losses due to the resistance of fingers and busbars can be controlled by designing the solar cell in an optimum manner. Increase the width of fingers and busbar can reduce the resistance associated with them. However, this leads to reduce the transparent area of the solar cell surface, and this causes shadowing losses as discussed previously (section 2.3.1). A high aspect ratio of fingers, i.e. tall fingers, can be used to limit both resistive and shadowing losses. Currently, screen print techniques are used for the metallisation processes of solar cell fingers (Antonini, 2003). These techniques give a high aspect ratio with reasonable cost.

Resistive losses owing to the solar cell emitter can also be mitigated by designing the emitter layer with larger width (increased thickness) and heavy doping. The sheet resistivity of the emitter is given by (Tao, 2014):

$$\rho = \frac{1}{q\mu_n N_D\, t} \qquad \text{Eq. (21)}$$

where q is the electron charge, μ_n is the electron mobility, N_D is doping density and t is the emitter thickness.

Notwithstanding, increase the doping level and width thickness of the emitter layer results in the reduced lifetime of minority carriers, as there is an increase in the probability of recombination mechanism as discussed previously. To minimise this effect, a thin emitter is required with low doping density. Therefore, the thickness and doping density of the emitter should be designed optimally to reduce both resistive and recombination losses. In order to reduce the resistance of the emitter, n-type semiconductors are normally used for the emitter layer. This is because the mobility of n-type semiconductors is higher than in p-type semiconductors (Tao, 2014).

The discussed resistances contribute to an increase in the series resistance, and hence limit the electrical output power. The fill factor is the performance indicator, which is mostly affected by the series resistance. It is estimated that 0.1Ω of the series resistance causes a reduction of the fill factor by approximately 2.5 (Dadu *et al.,* 2002).

The impact of the series resistance is more severe in large area solar cells. This is as a result of increased fingers length and the amount of current flow. Research and experiments have been carried out to investigate the accurate value of these resistances and their associated losses in order to produce more controllable solar cells. In 1982, Araujo proposed a good method to calculate the value of the series resistance by using the current-voltage curve of one diode and

one sun irradiance power. The equation of the current density (Equation 19) has been solved for the voltage as (Araujo and Marti, 1994):

$$J(V) = J_o(\exp\left(\frac{V + J\,R_S}{k_B\,T}\right) - 1) - J_{Ph} \qquad \text{Eq. (22)}$$

The area under the I-V curve (A)has been estimated, which presents the output power, by integrating the voltage from zero to the short-circuit current density (Pysch *et al.,* 2007).

$$A = \int_{J_2=0}^{J_1=J_{sc}} V(J)dJ \qquad \text{Eq. (23)}$$

Solving and simplifying this equation, series resistance can be written as (Pysch *et al.,* 2007):

$$R_{S,integral} = 2\left(\frac{V_{OC}}{J_{sc}} - \frac{A}{J_{SC}^2} - \frac{k_B\,T}{q}\cdot\frac{1}{J_{SC}}\right) \qquad \text{Eq. (24)}$$

Shunt resistance also limits the efficiency of solar cells, but in general, its impact is not as severe as that observed in series resistance. Shunt resistance occurs as a result of doping procedures, which leads to create defects. These defects create deep level states in the band gap (Van Dyk and Meyer, 2004). Low shunt resistance causes an alternative way for the generated current to leak from a solar cell (McMahon *et al.,* 1995). This reduces both the total generated current and the open circuit voltage, and in return reduces the solar cell efficiency. The issue of low shunt resistance becomes worse at low irradiance levels because the photocurrent produced from the solar cell is low (McMahon *et al.,* 1996; Van Dyk and Meyer, 2004).

Figure 9a displays the effect of increased series resistance (R_S) at constant shunt resistance on the I-V curve of a solar cell. It shows that the continuous increase of series resistance reduces the maximum output power until the solar cell is damaged at a resistance value of 300 mΩ. Figure 9b shows the impact of decreased shunt resistance at zero series resistance on a solar cell performance; the lowest shunt resistance value of 0.08 mΩ can destroy the solar cell, however, the highest value of 1000 mΩ results in a high output power (FÖll, 2011). Therefore, the ideal value for series resistance is zero and for shunt resistance is infinite.

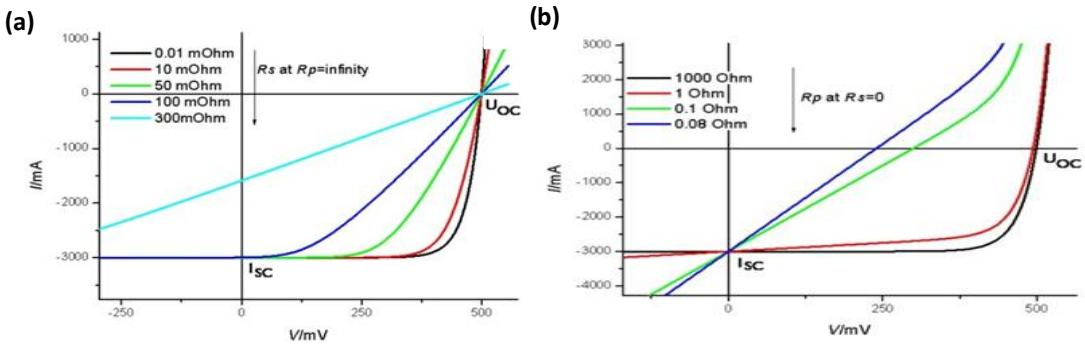

Figure 9: The influence of series and shunt resistances on solar cells performance.
(a) The impact of different values of series resistance on the I-V curve at infinite shunt resistance. (b) The impact of different values of shunt resistance at zero series resistance on the I-V curve (FÖll, 2011).

2.4 Solar Cell Based Amorphous Silicon

Amorphous silicon is a non-crystalline type of silicon semiconductor, where silicon atoms are ordered randomly. This random order leads to the high energy gap of about 1.7 eV (Boutchich, 2012). Each silicon atom bonds to only three other silicon atoms. Consequently, the fourth bond forms a dangling bond, which causes a defect in the lattice form (Böer, 2013). Such defects cause undesirable behaviours, which can limit the performance of solar cells. However, it is observed that the plasma deposition used to make amorphous silicon solar cells leads to the creation of hydrogen atoms (about 10% of the total Si atoms). Hydrogen atoms passivate the dangling bonds, and hence, reduce the unfavourable effects caused by their presence (Rech and Wagner, 1999). The hydrogenated amorphous silicon atomic structure is shown in Figure 10. The term 'hydrogenated amorphous silicon solar cell', a-si:H, is usually cited as 'amorphous silicon solar cell' (Deng and Schiff, 2003).

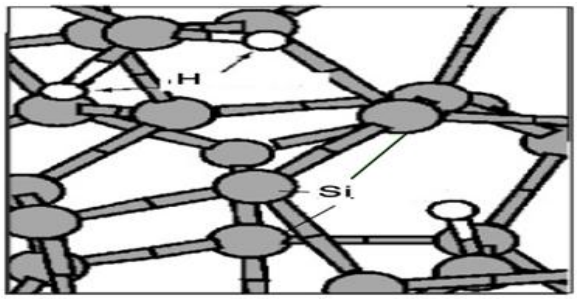

Figure 10: Atomic structure of hydrogenated amorphous silicon.
Gray spheres represent silicon atoms; white spheres represent hydrogen atoms where they bond to the silicon dangling bond (Deng and Schiff, 2003).

2.4.1 The Principal of Amorphous Silicon Solar Cell

The amorphous silicon solar cell consists of three thin layers: p-type, pure amorphous silicon, and n-type. These layers together create the photodiode of amorphous silicon solar cells. This type of photodiode is called p-i-n; the structure can be prepared in reverse order to generate an n-i-p photodiode. Most incident photons are absorbed in the intrinsic layer (the pure amorphous silicon without doping); therefore, the intrinsic layer is designed to be the thickest layer. Absorption of a photon leads to the creation of a free electron-hole pair, which will be separated by an electric field as can be seen in Figure 11 (Markvart and Castañer, 2012). The main difference between amorphous and crystalline silicon solar cells is that the generated carriers are collected by the electric field as a drift current instead of diffusion current in the former (Markvart and Castañer, 2012; Wronski and Carlson, 2001). Usually, a thin amorphous silicon photodiode is deposited on the substrate for supporting in either superstrate or substrate design. The design of the superstrate starts with a transparent substrate followed by a transparent conductive oxide, a photodiode and finally a reflector. On the contrary, the substrate design starts with a transparent conductive oxide followed by a photodiode, a reflector and finally a substrate (Hegedus and

Shafarman, 2004; Böer, 2013). These different designs are purpose built. For example, the superstrate is usually used for architectural glass buildings, whereas the substrate design is used for producing flexible solar cells for different applications.

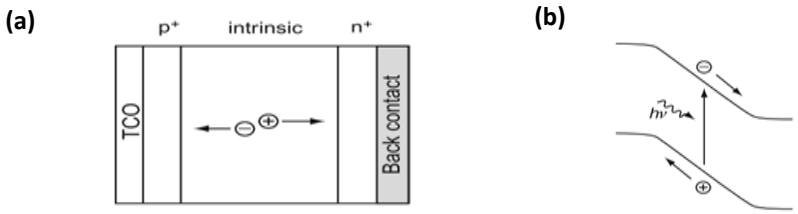

Figure 11: The operation of amorphous silicon solar cells.
(a) The physical structure of a p-i-n photodiode, showing light absorption and carrier generation in the intrinsic layer. (b) The operation process on the band energy levels. These processes occur in the intrinsic layer and the generated carriers are collected by the back contact and the transparent conductive oxide (TCO) (Markvart and Castañer, 2012).

2.4.2 The Potential of Amorphous Silicon Solar Cell

The high electrical features of amorphous silicon deposited as a thin film, in the form of silane (SiH_4) gas discharge, were brought to light in 1973 by Spear and LeComber (Deng and Schiff, 2003). This deposition method is commonly known as plasma enhanced chemical vapour deposition (PECVD) (Böer, 2013). In 1975, they found that doping silane with phosphine (PH_3) or diborane (B_2H_6) gas enhanced the electronic properties of the amorphous silicon solar cell. One year later, Carlson and Wronski presented an amorphous silicon solar cell with an efficiency of about 2.4%. They concluded that making amorphous silicon solar cells by plasma deposition gave better efficiencies than using classical methods such as evaporating silicon. Figure 12 shows the current density *versus* voltage curve of the Carlson and Wronski single junction amorphous silicon solar cell and a triple junction amorphous silicon cell reported in 1997, the latter of which had an improved efficiency of 6 times greater than the former (Deng and Schiff, 2003).

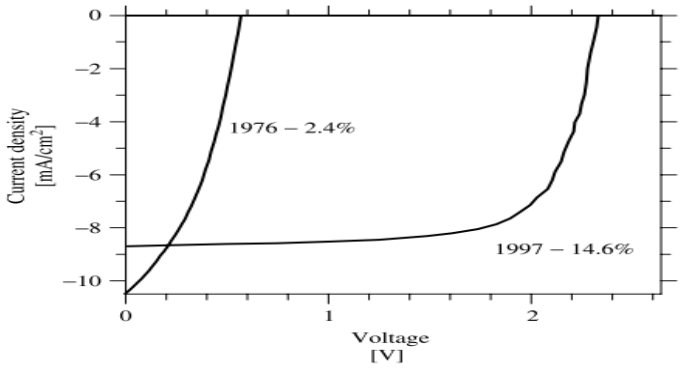

Figure 12: Current density-voltage curve of Carlson and Wronski single junction and triple junction amorphous silicon solar cells.
The Carlson and Wronski single junction amorphous silicon reported in 1976 showed an efficiency of 2.4% whilst the triple junction silicon presented in 1997 gave an efficiency of 14.6% (Deng and Schiff, 2003).

Amorphous silicon is a profitable field for solar cells due to many features. The property of light absorption of amorphous silicon solar cell is about 40 times higher than that of crystalline silicon solar cells since it has a higher absorption coefficient (Mah, 1998). Figure 13a shows the difference of the absorption coefficient α (m^{-1}) of the crystalline and the amorphous silicon solar cell as a function of photon energy hυ (eV). The absorption coefficient of both solar cells increases with photon energy until 2.5 eV. For example, blue light is usually absorbed near the solar cell surface due to its high energy (Hegedus and Shafarman, 2004; Rech and Wagner, 1999). The high absorption coefficient enables amorphous silicon solar cells to absorb a high amount of incident light. The amorphous silicon solar cell has an advantage of the direct band gap, which allows it to absorb a significant amount of incident light in a very limited (micrometre) thickness (Fritzsche, 2001). Additionally, the energy gap of amorphous silicon, which is about 1.7 eV, can easily be varied. To increase the energy gap, amorphous silicon can be mixed with carbon or oxygen; however, to decrease the band gap, it can be alloyed with germanium. Being able to vary the energy gap has enhanced the development of tandem solar cells (Böer, 2013; Rech and Wagner, 1999).

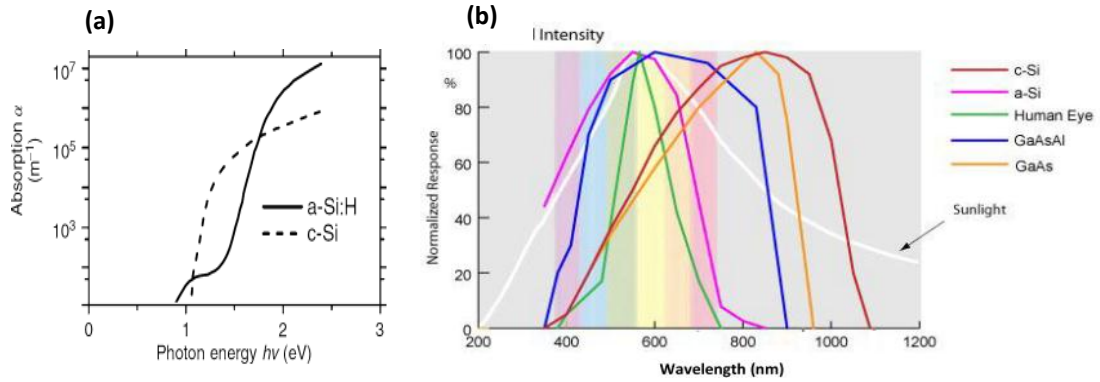

Figure 13: The absorption coefficient and the spectral response of amorphous silicon solar cell.
(a) Absorption coefficient α (m^{-1}) with respect to incident photon energy hυ (eV) of crystalline silicon (dashed line) and amorphous silicon (black line). Amorphous silicon has a higher absorption coefficient (about 10^7 cm^{-1}) at 2.5 eV; whereas, the absorption coefficient of crystalline silicon is 10^6 m^{-1} (Böer, 2013). (b) The response of different solar cells over the solar spectrum. The pink curve shows the response of amorphous silicon; it reaches the highest value in the visible light region. The red curve presents the response of crystalline silicon; it reaches the highest response in the near infrared region.
(http://www.greenrhinoenergy.com/solar/technologies/pv_cells.php)

Moreover, amorphous silicon solar cells show a good response in the visible light region. Figure 13b shows the response of amorphous silicon and other types of solar cells in different regions of the solar spectrum. As can be seen from the curve, the sensitivity of the amorphous silicon solar cell in the visible light region is much closer to the sensitivity of human eyes to the sunlight. For this reason, amorphous silicon is widely used in light sensor technologies (SANYO Semiconductor Co., Ltd. Website, 2007). In spite of the fact that crystalline silicon solar cells respond to a wide band of the solar spectrum, the sensitivity of the amorphous silicon solar cell outweighs that of crystalline silicon solar cells in the visible light region. This gives the former an advantage since the

visible light region has the highest spectral intensity of the solar spectrum (Green rhino energy). However, due to the fact of defect states in amorphous silicon solar cells, recombination losses highly occur comparing to crystalline silicon solar cells, and this can lead to a reduction in the carriers' lifetime, and hence, reduced solar cell efficiency (Hegedus and Shafarman, 2004).

2.4.3 Staebler–Wronski Effect

Defects exist in amorphous silicon solar cells due to dangling bonds. To reduce the density of dangling bonds in amorphous silicon solar cells, hydrogen atoms are doped into the solar cell. However, during the first hundred hours of light soaking, the silicon-hydrogen bonds are broken leading to an increase in defect density. Consequently, deep level states are created in the band gap, which increases the probability of electron-hole pair recombination. The phenomenon of decreased efficiency as a result of light interaction is known as the Staebler–Wronski Effect (Radue and Dyk, 2010). This effect plays an important role in efficiency degradation of amorphous silicon solar cells. The efficiency degradation of a single junction amorphous silicon solar cell due to the Staebler–Wronski Effect has been estimated as 30% of the starting efficiency. The degradation issue is less problematic in triple junction amorphous silicon solar cells as it is estimated to be 15% (Deng and Schiff, 2003; Radue and Dyk, 2010; Guha *et al.,* 2000; Böer, 2013). Generally, after the first hundred hours, the solar cell output power becomes more stable as shown in Figure 14. The metastable degradation can be practically mitigated by thermal annealing up to 160°C for a few minutes (Böer, 2013; Deng and Schiff, 2003).

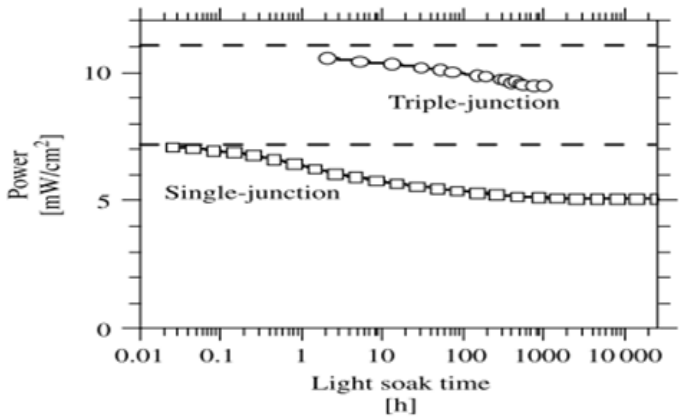

Figure 14: The Staebler–Wronski Effect on the performance of a single and a triple junction a-si:H solar cells under a solar simulator (100 mW/cm^2).The stability of the efficiency with respect to light exposure is reached after about a hundred hours (Deng and Schiff, 2003).

2.4.4 Literature Review

There is a large volume of research papers describing the impact of light absorption, light trapping, and deposition methods on the performance of amorphous silicon solar cells.

Defects resulting from light soacking play a significant role in enhancing electron-hole pair recombination in amorphous silicon solar cells. Therefore, to reduce electron-hole pair

recombination, generated electron-hole pairs in the intrinsic layer should be collected quickly. This can be achieved by reducing the thickness of the intrinsic layer; thus, generated carriers travel a shorter distance to reach an electrode where they can be collected (Rech and Wagner, 1999). However, a thinner intrinsic layer reduces photon absorption probabilities, and hence, reduces generated electron-hole pairs. To enhance photon absorption in thinner layers, a light-trapping mechanism has been developed by adopting a top textured surface and a back reflector (Liu *et al.,* 2014).

Long wavelengths are weakly absorbed by amorphous silicon solar cells, as they do not have a capable energy to excite electrons. Hence, the spectral response and the quantum efficiency of amorphous silicon solar cells in the near infrared region are poor. Hegedus et al. (1996) investigated the impact of a back reflector and a textured surface in enhancing the performance of an amorphous silicon solar cell with a thickness of 250 nm. It was found that the quantum efficiency showed an improvement in the near infrared region by a double while in the blue region it shows a slight improvement (Böer, 2013).

Amorphous silicon thin films can be prepared by many different deposition techniques (Böer, 2013). The technique of plasma enhanced chemical vapour deposition at very high frequency (VHF-PECVD) has been used in many studies, which resulted in good solar cell performance (Smets *et al.*, 2008; Takatsuka *et al.*, 2004; Fujioka *et al.*, 2006). Recent evidence suggests that the inductively coupled plasma chemical vapour deposition (ICP-CVD) method can give a high quality solar cell with low cost (Huang *et al.*, 2012). Huang *et al.* (2012) examined the performance of two heavily doped pin amorphous silicon solar cells with the same thickness prepared by different deposition techniques, VHF-PECVD and ICP-CVD. Current density-voltage curves of both solar cells were examined, as shown in Figure 15a. The results showed that the solar cell grown by ICP-CVD resulted in a high power conversion efficiency of 9.6% with the short circuit current density and open circuit current voltage of 15.7 mA/cm^2 and 0.91 V, respectively. However the solar cell grown by VHF-PECVD gave an efficiency of 8.8% with the short circuit current density and open circuit voltage of 14.2 mA/cm^2 and 0.92 V, respectively. The measured quantum efficiency $QE(\lambda)$ curve of both solar cells extends from 300-750 nm as shown in Figure 15b. The only difference is that the $QE(\lambda)$ of the ICP-CVD solar cell moves to a certain extent towards the red region. The reason behind this difference was suggested as a result of low hydrogen density of the ICP-CVD solar cell in comparison to the VHF-PECVD solar cell. The hydrogen density plays an essential role in determining the band gap and the optical absorption of amorphous silicon solar cells; the gap increases with hydrogen density while the optical absorption decreases (Qin *et al.*, 2010). This suggestion is agreed with the band gap measurement profile as it was found that the band gap of the ICP-CVD solar cell and the VHF-PECVD solar cell are 1.85 eV and 1.90 eV, respectively.

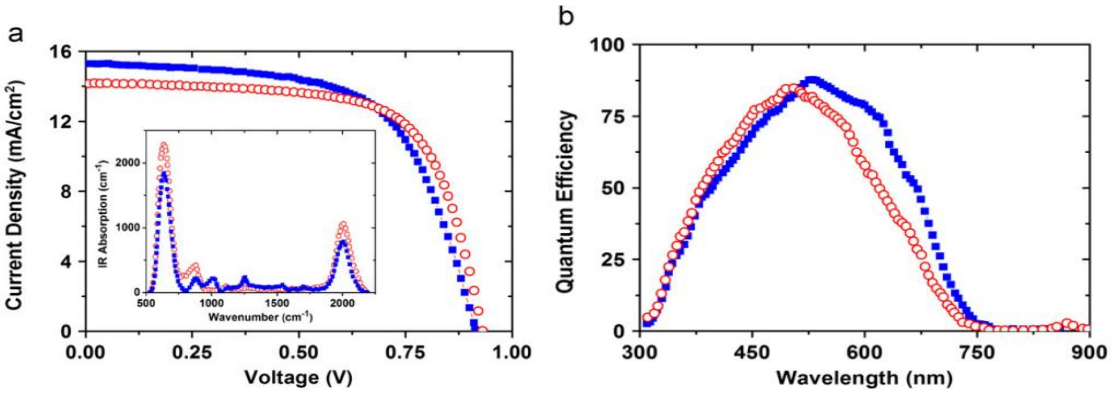

Figure 15: Performance comparison between ICP-CVD and VHF-PECVD amorphous silicon solar cell.
(a) Current density with respect to voltage for the ICP-CVD (blue) and VHF-PECVD (red) amorphous silicon solar cells. Both devices have a similar V_{OC}; however the I_{SC} of ICP-CVD device is higher. (b) Quantum efficiency with respect to photon wavelength (blue) and VHF-PECVD (red) amorphous silicon solar cells. Both curve start and cut-off at the same wavelength, however, ICP-CVD solar cell gives more efficient improvement in near infrared region (Huang et al., 2012).

3 Methodology

This chapter presents the methodology that was followed to accomplish the aim of this project. An experiment was carried out to estimate the power conversion efficiency and the spectral power efficiency of both an amorphous silicon solar cell and a standard crystalline solar cell. The power conversion efficiency of both types of solar cells illuminated by the entire solar spectrum AM0 was calculated and analysed at different wavelength bands. The experiment was carried out to measure the photocurrent against bias voltage. Six measurements were performed for both solar cells; one under the entire solar spectrum AM0 and the remaining measurements were carried out under particular wavelength bands using filters.

3.1 Experiment requirements

In order to conduct the experiment on solar cells, three types of equipment were used. The crystalline silicon solar cell was used as a reference solar cell and the amorphous silicon solar cell was used as a test solar cell. A solar simulator was utilised to illuminate both solar cells. Then, the generated photocurrent was measured by a picoammeter, which automatically sends the observed data to a computer, which in turn plots the current *versus* voltage curve in a lap view. The measurement structure is displayed in Figure 16.

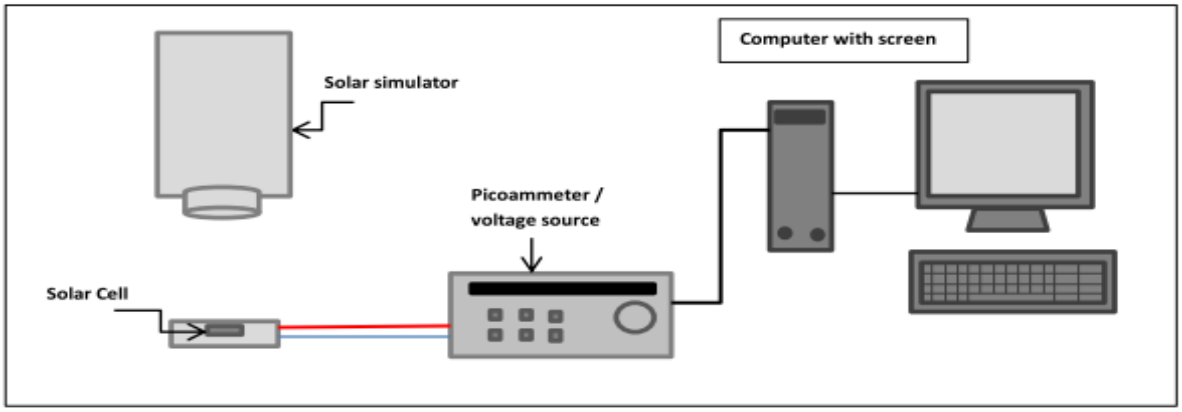

Figure 16: The layout of the current *versus* voltage experiment.
The solar simulator illuminates the solar cell while the solar cell is connected to a digital picoammeter. The digital picoammeter measures the produced photocurrent *versus* voltage. The current-voltage data is sent to a computer supported with a lab view program, which displays the current-voltage curve.

Solar Simulator:

An Oriel SoI3A solar simulator with a Xenon source of Newport corporation brand was used to illuminate solar cells. The solar source provides a solar spectral irradiance approximated to the standard solar radiation. The solar spectrum assumed in this measurement is equivalent to the extraterrestrial irradiance spectrum known as 'air mass zero' (AM0) solar spectrum. The solar simulator is supported by a power meter, which measures the total integrated irradiance in the unit of sun. The solar spectral irradiance AM0, according to the National Renewable Energy

Laboratory (NREL), can be plotted in the unit of W/m^2 as a function of wavelength in the unit of µm as shown in Figure 17. The power of the total integrated irradiance is equal to 1 sun (the solar constant is equivalent to 1366.1 W/m^2).

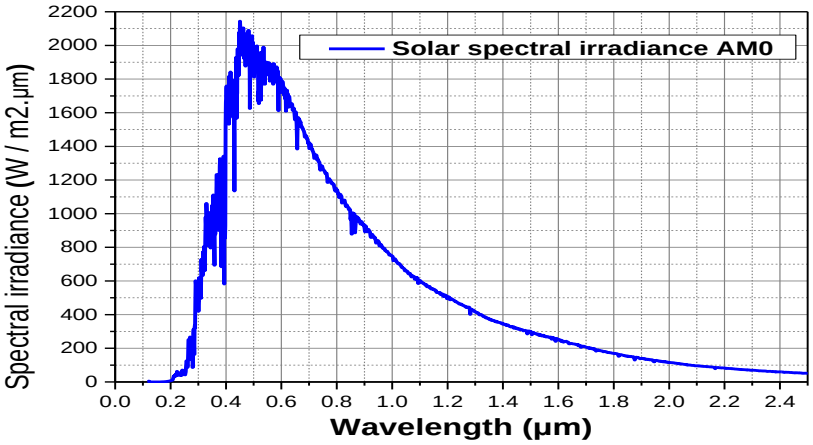

Figure 17: Extraterrestrial spectral irradiance *versus* wavelength.
(Data obtained from Renewable Resource data Energy Centre, NREL, US Department of Energy).

Picoammeter/ Voltage source

A KEITHLEY 489 picoammeter device was used in the experiment to measure the photocurrent and voltage and to provide a voltage supply. Start and stop bias voltage were manually managed for each measurement and the photocurrent corresponding to bias voltage was automatically measured and sent directly to a computer with a lab view program. The computer is provided by C-V/I-V Measurement Software to plot the current-voltage curve.

Filters

Five filters were used to determine the efficiency of both solar cells in particular wavelength bands of the solar spectrum. Each filter transmits a known wavelength band of the solar spectrum with a spectral irradiance limit. Two filters transmit particular wavelength bands of near infrared radiation while one filter passes a wavelength band of ultraviolet radiation. The remaining filters pass different wavelength bands of visible radiation. Table 1 presents the centre wavelength, the full width band, and the peak transmission of used filters.

Table 1: The approximated width band and transmission data of filters.
(Data: from Thorlabs website for all filters except L-514.5 from TFI technology Thin Film Imaging website).

Filters	Centre wavelength (nm)	Full width band (nm)	Transmission (%)
FB390-10	390 ± 2	10 ± 2	30
FB470-10	470 ± 2	10 ± 2	45
L-514.5-10	514.5± 2	10 ± 2	65
FB530-10	350 ± 2	10 ± 2	25
FB730-10	730 ± 2	10 ± 2	50
FB880-40	880 ± 8	40 ± 8	70

Solar Cells Samples

The n-type crystalline silicon used as a reference solar cell is Photoconductive Solderable Chip (S-25CL/VL), which has a standard typical specification. The test cell is n-type amorphous silicon consisting of about six photodiodes.

3.2 Experimental procedure

The current-voltage curve characteristics of both the crystalline and amorphous silicon solar cells were obtained with and without filters. The total input power from the solar simulator was measured, which gave the total integrated intensity of the solar spectrum of 1 sun.

Measurement of the crystalline silicon solar cell

Firstly, in order to measure the photocurrent *versus* voltage under the entire solar spectrum AM0, the crystalline silicon solar cell was placed on a holder where it could be illuminated by the solar simulator as shown in Figure 16. A small area of the solar cell surface of 1.77 mm^2 was chosen as a sample. The area size was fixed by placing a mask with a small hole on the top of the solar cell. The start and stop bias voltage were applied as -1 V and +1 V, respectively. Thereafter, the generated photocurrent corresponding to the bias voltage for the integrated solar cell was shown on the lap view program.

Secondly, to determine the spectral power efficiency of the crystalline silicon solar cell, the photocurrent *versus* voltage was measured under particular wavelength bands. In order to achieve this, filters were individually placed at the top of the solar cell. Current *versus* voltage measurements of the solar cell with filters were carried out using the following protocol:

1) The FB390 filter was used to pass ultraviolet radiation in the wavelength band from about 385 to 395 nm. Since the photocurrent was high for the ammeter, the bias voltage was managed from -1 to + 0.5 V.
2) The FB470 filter was used to pass a wavelength band from about 465 to 475 nm. The start and stop bias voltage were not changed.
3) The third filter L-514.5 was used to measure the solar cell performance in the visible region of the solar spectrum. It passes the wavelength band from about 508 to 520 nm. The start and stop bias voltage were fixed from -1 to +1 V.
4) To estimate the solar cell performance in the near infrared region, a FB730 filter was applied on the top of the solar cell. This filter transmits near infrared wavelengths from 725 to 735 nm. The bias voltage was not change, i.e. from -1 to +1 V.
5) The last filter was used to determine the efficiency of the solar cell in the near infrared region. The FB880 filter was used to measure the photocurrent *versus* voltage in the wavelengths ranging from 870 to 890 nm. The start bias voltage was set on -1 V and the stop bias on +1 V.

The measurement of the amorphous silicon solar cell

The photocurrent of the amorphous silicon solar cell was measured following the same steps as that used for the crystalline silicon solar cell measurement. However, the area of the amorphous silicon solar cell was increased to 35 mm^2 due to its lower performance and further, the bias voltage was extended.

Firstly, the current *versus* voltage measurement of the solar cell was carried out over the entire solar spectrum AM0 (without a filter) where the bias voltage was set from -5 to +5 V. Secondly, the current *versus* voltage measurement was performed at different wavelength bands of the solar spectrum using the same filters. For all measurements with filters, the bias voltage was fixed from 0 to +5 V.

4 Analysis

This chapter analyse the data obtained from each measurement of both types of silicon solar cells. Current-voltage curves were plotted to estimate the maximum output power. The maximum output power and the input power were estimated for each measurement, and hence, the power conversion efficiency of solar cells was calculated. The chapter also presents a comparison between the spectral power efficiency of both the crystalline silicon solar cell and the amorphous silicon solar cell.

The maximum output power from the current-voltage curve is estimated as the knee point of the curve. However, the plot of the generated power as a function of the bias voltage in the same graph makes the estimation of the maximum current, maximum voltage, and maximum output power more accurate. The power-voltage curve is obtained by multiplying the generated photocurrent by the bias voltage.

The performance of the crystalline silicon solar cell was normal and the current-voltage curve was smooth as shown in Figure 18a. The estimated maximum output power is 0.000126 W. To determine the efficiency of the crystalline silicon illuminated by the entire solar spectrum AM0, the maximum output power was divided by the solar irradiation power over the solar cell surface. The total power of the incident light from the solar simulator is equal to 1366.1 W/m^2 and the area of the solar cell is 1.77 mm^2. Hence, the efficiency of the crystalline silicon solar cell was calculated by using the equation (4) as:

$$\eta_{Xtal} = \frac{1.26\times 10^{-4}(W)}{1366.1\ (W/m^2)\times 1.77\times 10^{-6}\ (m^2)} = 5.210\ \%$$

The efficiency is quite low comparing to the industrial silicon solar cells which produce electricity with an efficiency of 15-18% (Saga, 2010). This is because the crystalline silicon solar cell that was used is a photodiode with a small illuminated area, which was chosen randomly.

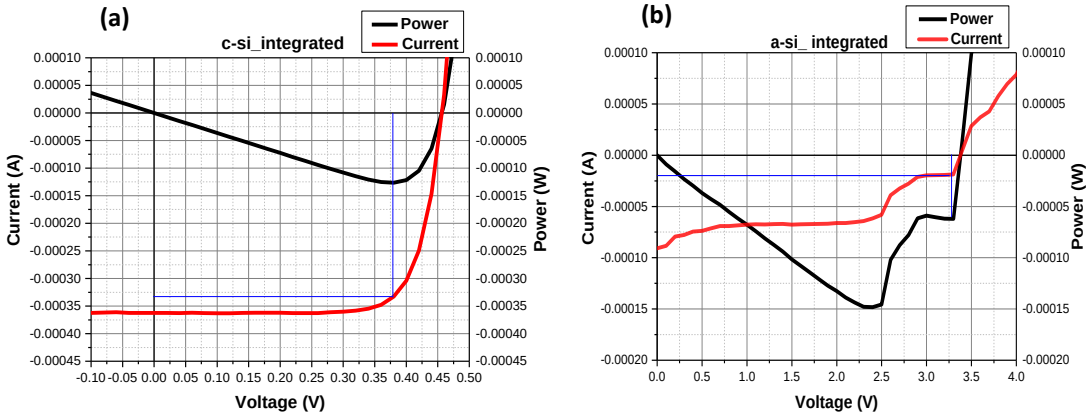

Figure 18: Current *versus* voltage measurements of the integrated c-si and a-si solar cells.
The performance curves of (a) the crystalline silicon (c-si_integrated) and (b) the amorphous silicon (a-si_integrated) measured over the integrated solar spectrum. The red curve shows the current *versus* voltage whilst the black curve shows the produced power *versus* voltage. The maximum power point of the I-V curve is estimated by projecting a line from the maximum power point of the power curve to the current curve. The knee point is where the line intersects the current curve. The current- voltage curve of the amorphous cell shows more than one prominence. The maximum power point is estimated at the second knee point of the current-voltage curve.

Interestingly, the amorphous silicon solar cell showed an unusual current-voltage curve. As seen in Figure 18b, there are two points, which could relate to the maximum power point. This may occur as a result of the fact that the amorphous silicon solar cell consists of more than one photodiode and the illuminated area was chosen randomly. It is assumed that the last knee point is the maximum power point, which gives about 0.00014 W of electrical power. The efficiency of the illuminated amorphous silicon solar cell (35 mm^2) under the total solar spectrum was calculated using equation (4) as:

$$\eta_{Alpha} = \frac{0.00014\ (W)}{1366.1\ (W/m^2) * 35 \times 10^{-6}\ (m^2)} = 0.293\ \%$$

The measured efficiency (0.293%) of the amorphous silicon solar cell is very low comparing to the efficiencies of manufactured amorphous silicon solar cells which are in the range 6-9% (ENERGY.GOV).

To determine the spectral power efficiency of both solar cells, the power conversion efficiency of both solar cells over particular wavelength bands were analysed. In order to accomplish this, the total input power of the solar radiation through each filter along with the maximum output power was estimated.

Similar procedures that were used to obtain the maximum output power of the integrated measurements were followed for all measurements (with filters) for both solar cells. The current *versus* bias voltage curves of the crystalline cell resulting from each filter are shown in Figure 19.

The current-voltage curves of all crystalline solar cell measurements are smooth. As a result, the performance parameters of the crystalline silicon were clearly identified. The different performance factors which include maximum current (I_m), maximum voltage(V_m), short circuit current(I_{SC}), open circuit voltage(V_{OC}), and maximum power (P_{Max}) are presented in Table 2.

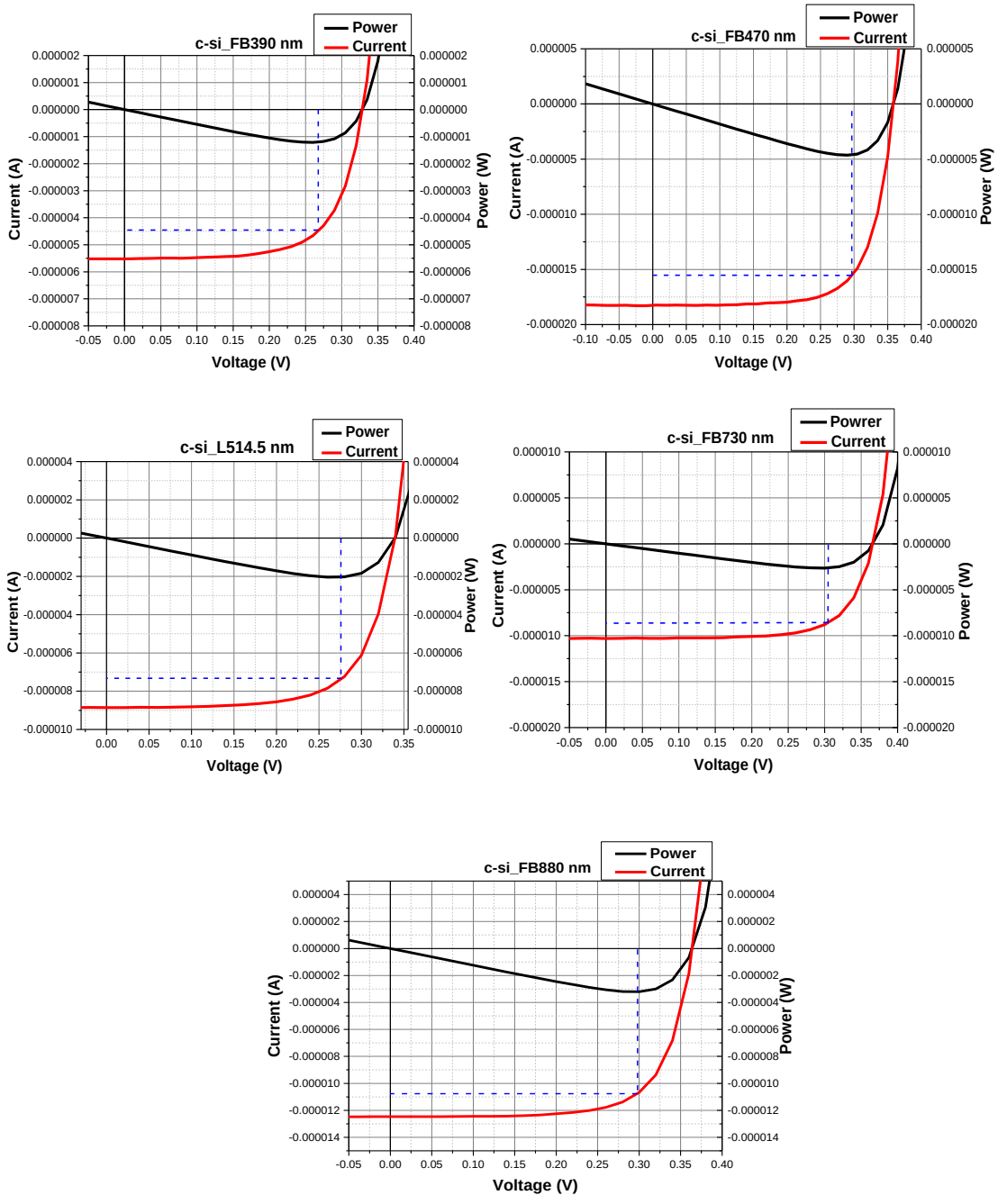

Figure 19: The current-voltage (red) and the power-voltage (black) curves for the crystalline silicon solar cell (c-si) illuminated by different wavelengths.
The I_m and V_m are intersection points of the blue line with the y- and x-axis, respectively.

Table 2: The performance parameters of the crystalline silicon solar cell extracted from different measurements of different filters.

Filters	I_m (A)	V_m (V)	I_{SC} (A)	V_{OC} (V)	P_{Max} (W)
FB390 nm	0.4456×10^{-5}	0.266	7.19×10^{-6}	0.327	1.1853×10^{-6}
FB470 nm	0.155×10^{-4}	0.296	1.82×10^{-5}	0.36	4.588×10^{-6}
L-514.5 nm	0.732×10^{-5}	0.275	8.9×10^{-6}	0.34	2.013×10^{-6}
FB730 nm	0.87×10^{-5}	0.299	1.02×10^{-6}	0.365	2.623×10^{-6}
FB880-40 nm	0.108×10^{-4}	0.297	1.24×10^{-5}	0.363	3.2076×10^{-6}

Using the data in Table 2, the performance of the crystalline silicon solar cell over the integrated solar spectrum and over particular wavelengths can be compared. The maximum power generated from the solar cell is the key parameter for comparison. The power contribution of each filter is given as the maximum output power resulting from the wavelength band of the filter divided by the maximum power generated from the integrated solar irradiance (1.26×10^{-4} W). The power produced from the crystalline silicon solar cell under ultraviolet wavelengths (from 385 to 395 nm) is just about 0.94% of the total power under the whole solar spectrum. This small amount is because most of the ultraviolet energy is lost as thermal energy due to its excessive energy comparing to the energy gap of the crystalline silicon solar cell. Additionally, the input power of ultraviolet light, which could be converted to electrical power, is lower than that of visible light since ultraviolet light has a lower spectral irradiation. When the incident light is in the range of 466 to 476 nm, the crystalline silicon solar cell can produce 3.64 % of the total integrated output power. The crystalline silicon solar cell can generate about 1.6 % of the total integrated output power when the incident light in the range of 509 to 519 nm. These findings agreed with the theoretical spectral response of the crystalline silicon solar cell, as the output power improves under visible radiation. Near infrared radiation (wavelength 725 to 735 nm) is converted to electrical power creating about 2 % of the total output power of the integrated crystalline silicon solar cell. Longer wavelength radiation (875 to 885 nm) is converted to electrical power, which forms about 2.55 % of the maximum output power generated by the integrated solar cell.

The photocurrents produced by the amorphous silicon solar cell at different incoming wavelength bands are plotted with respect to the bias voltage in Figure 20.

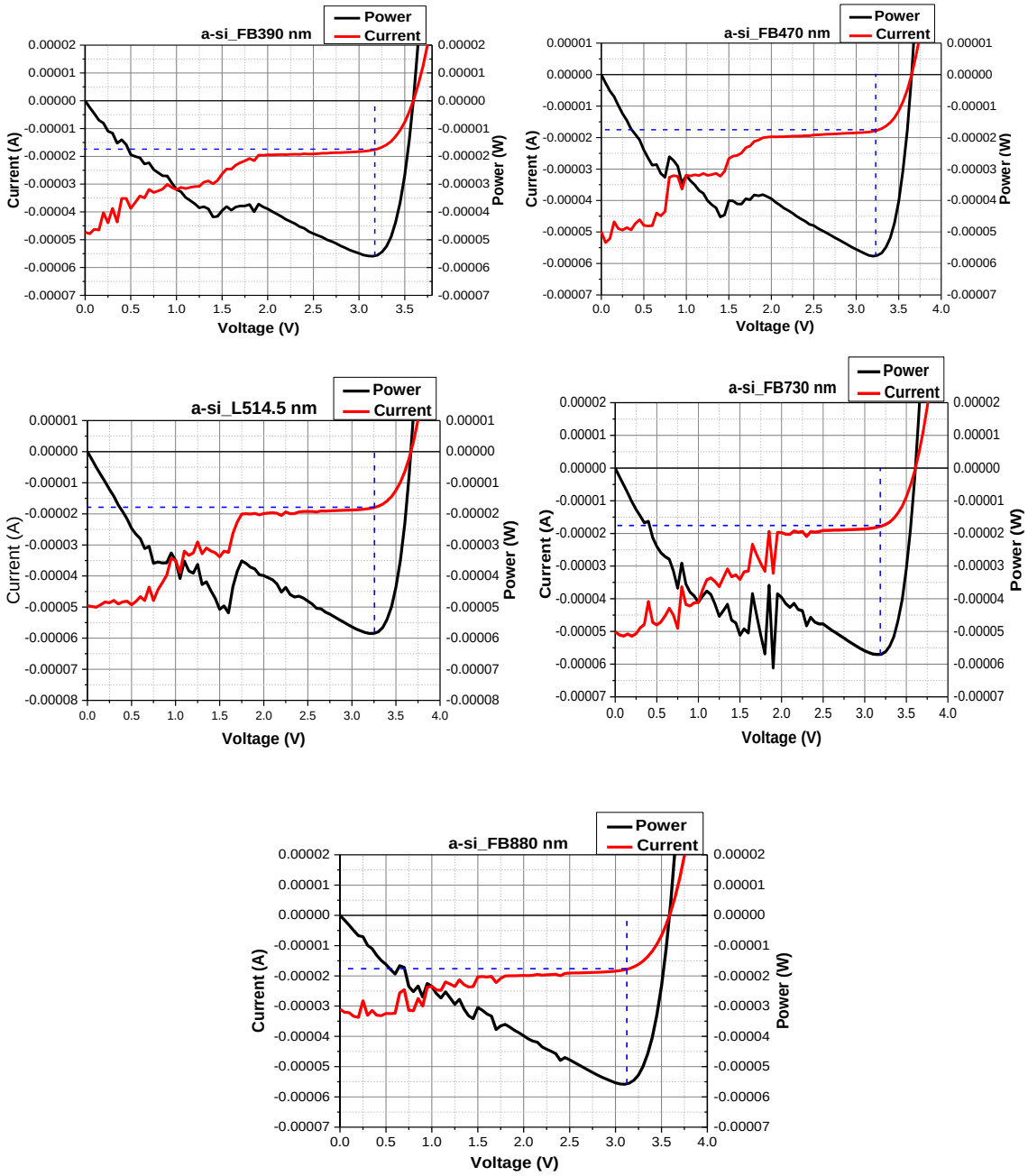

Figure 20: Current-voltage curve of the amorphous silicon solar cell illuminating through filters.

At the beginning of each curve, the amorphous silicon solar cell draws a fluctuating current. This may be due to the fact that the amorphous silicon solar cell consists of a number of photodiodes and only 35 mm^2 of a randomly chosen area was exposed. The zigzag curve makes an accurate estimation of the short circuit current difficult. Nevertheless, the maximum output power is the main focus in this experiment.

In order to obtain the short circuit current, the fluctuating parts of the current-voltage curve are assumed smooth. Hence, the short circuit current values of the amorphous silicon solar cell for

the five measurements are based on this assumption. The parameters that indicate the performance of the amorphous silicon solar cell I_m, V_m, I_{SC}, V_{OC}, and P_{Max} are shown Table 3.

Table 3: The parameter of current –voltage curves of the amorphous silicon solar cell resulting from different wavelength bands of the solar spectrum.

Filters	I_m (A)	V_m (V)	I_{SC} (A)	V_{OC} (V)	P_{Max} (W)
FB390 nm	1.73×10^{-5}	3.16	1.9×10^{-5}	3.6	5.4668×10^{-5}
FB470 nm	1.75×10^{-5}	3.22	1.9×10^{-5}	3.65	5.635×10^{-5}
L-514.5 nm	1.77×10^{-5}	3.25	2×10^{-5}	3.67	5.7525×10^{-5}
FB730 nm	1.76×10^{-5}	3.18	1.9×10^{-5}	3.6	5.5968×10^{-5}
FB880-40 nm	1.74×10^{-5}	3.12	2×10^{-5}	3.58	5.4288×10^{-5}

It seems that the amorphous silicon solar cell, illuminated by different wavelength bands of the solar spectrum, produced approximately the same amount of power. The amorphous silicon solar cell produces a higher amount of power in the visible light region. This is because the ability of amorphous silicon solar cells in converting light into electricity reaches its highest in the visible light region.

To evaluate the power conversion efficiency of the crystalline and amorphous silicon solar cells at particular wavelengths, the input power through each filter was calculated. Referring back to the solar spectrum AM0 (Figure 17), the total input power of the entire solar spectrum AM0 is given by the integral of the solar spectral irradiance as a function of the photon wavelength over the entire solar spectrum from zero to infinity. This means that the input power of the entire solar spectrum AM0 is defined as the total area under the solar spectral irradiance curve. It is assumed that the area under the curve from 200 to 2500 nm is equal to the total input power, which has been measured at 1366.1 W/m^2. This area is divided to small squares; hence, the total area under the curve (A_{tot}) was estimated by summing the total number of the small squares under the curve. It was found that the total area under the solar spectral irradiance curve equals to 2711.5 squares. Each filter passes a portion of solar wavelengths with a transmission limit. The transmission percentages with respect to the wavelength band of these filters are shown in Figure 21. The shape of each curve was reshaped to a rectangular shape (shown in red) to simplify the area calculation of the transmission curve of each filter. Thus, the effective area that represents the incident power through each filter is the ratio of the area under the transmission curve (A_f) (the rectangular shape) over the total area under the solar spectral irradiance curve (A_{tot}) multiplied by the transmission value (T) of the filter.

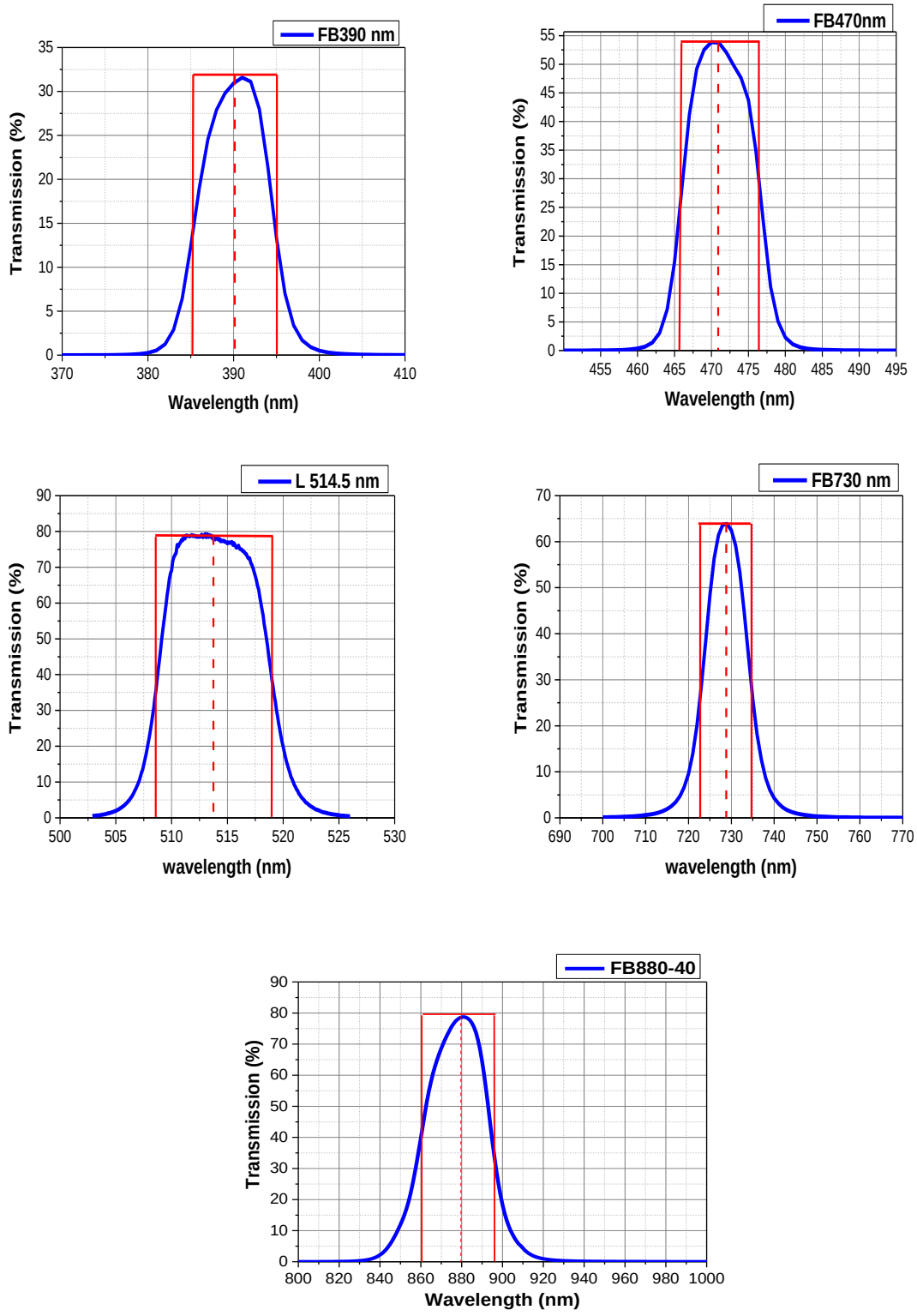

Figure 21: Spectral transmission curve for each of the filters.
The red rectangle is the estimation area of the input power of the filters (Data: Thorlabs website).

The wavelength bands of these filters comparing to the whole solar spectrum AM0 are shown in Figure 22. To determine the input power of each filter in the unit of W/m^2, the proportion area of each filter was multiplied by the real input power of the integrated solar spectral irradiance (1366.1 W/m^2). Hence, the input power of these filters could be written as:

$$P_{in\_filter} = \frac{A_f}{A_{tot}} \times T \times 1366.1 \left(\frac{W}{m^2}\right)$$

where A_{tot} equals to 2711.5 squares and the transmission value (T) is varied depending on filters. The calculation of the input power of the filters is shown in Table 4.

Table 4: Input power of solar light through filters.
Note: the transmission value here is based on the value shown in the transmission curve of the filters – Figure 19.

Filters	A_f (squares)	T (%)	P_{in} (W/m^2)
FB390	13.5	31.75	2.159
FB470	42	54	11.427
L-514.5	38.5	79	15.324
FB730	31.2	64	10.04
FB880-40	69	79	27.45

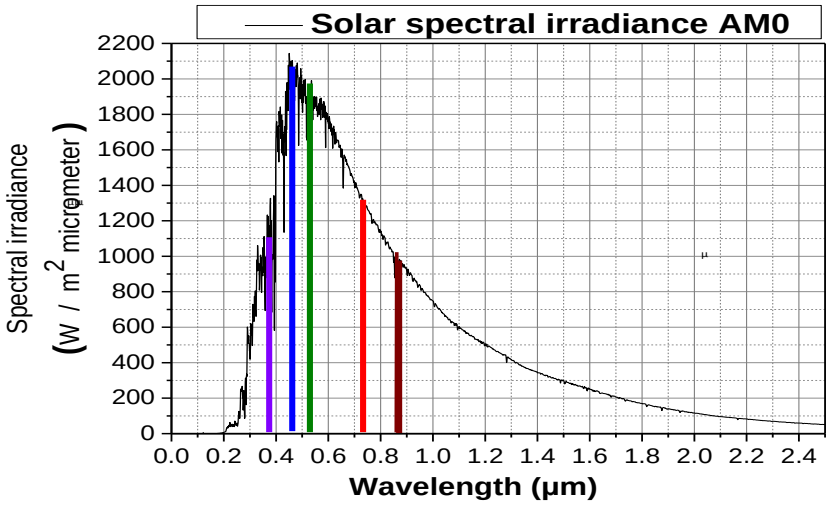

Figure 22: Input power of filters in comparison to the entire solar spectral irradiance AM0.
Each colour indicates the input power of different filters (FB390 = purple, FB470 = blue, L-514.5 = green, FB730 = red and FB880 = maroon). The filters could not transmit the whole power of the radiation; they transmit a limited percentage of the spectral irradiance.

Hence, the power conversion efficiency of both the crystalline silicon and amorphous silicon solar cells was calculated by using Equation 4. The next table displays the estimated efficiency of both solar cells with respect to the central wavelength of each filter. The illuminated surface area of the crystalline and amorphous silicon cells are 1.77 mm^2 and 35 mm^2, respectively.

Table 5: The efficiency of the crystalline and amorphous silicon solar cells resulting from wavelength bands through filters.

Filters	P_{in} (W/m^2)	Crystalline silicon solar cell			Amorphous silicon solar cell		
		P_{in} (W)	P_{output} (W)	Efficiey (%)	P_{in} (W)	P_{output} (W)	Efficiency (%)
FB390	2.159	3.82×10^{-6}	1.185×10^{-6}	31.02	7.56×10^{-5}	5.4668×10^{-5}	72.35
FB470	11.427	2.02×10^{-5}	4.588×10^{-6}	22.68	3.99×10^{-4}	5.635×10^{-5}	14.09
L-514.5	15.324	2.71×10^{-5}	2.013×10^{-6}	7.42	5.36×10^{-4}	5.7525×10^{-5}	10.73
FB730	10.04	1.78×10^{-5}	2.623×10^{-6}	14.76	3.514×10^{-4}	5.5968×10^{-5}	15.93
FB880-40	27.45	4.86×10^{-5}	3.2076×10^{-6}	6.60	9.61×10^{-4}	5.4288×10^{-5}	5.65

The results, as shown in Table 5, indicates that the amorphous silicon solar cell gives better performance in the ultraviolet radiation region comparing to the crystalline silicon solar cell. Although the former is able to convert ultraviolet light into electricity more efficiently than the latter, the recorded efficiency of 70% is highly excessive. It breaks the Shockley–Queisser limit where the theoretical maximum efficiency of a single junction amorphous silicon solar cell is about 29 % (Tao, 2014). Such an inaccurate result may be due to random errors that are encountered in the measurements. Another possible explanation for this might be due to the assumption that the integrated spectral irradiance (1 Sun) is equivalent to the area under the solar spectral irradiance curve of only 200 to 2500 nm; in actual fact, the spectral irradiance extends from zero to infinity wavelength. However, the solar spectral irradiance in the solar spectrum from 200-2500 nm is about 96.3% of the total spectral irradiance (Newport.com). The estimation of the solar input power through filters using the Planck equation might provide a more accurate result, as it was found that the Planck spectrum at 5800 K has a very similar curve to the solar spectral irradiance AM0 curve (Soffer and Lynch, 1999). The Planck equation $B_\lambda(T)$ defines the irradiance by a blackbody (F) as a function of the wavelength at a temperature of 5800K and is given by:

$$F = \pi \int_0^\infty B_\lambda \ (T)\, d\lambda = \int_0^\infty \pi \frac{2hc^2}{\lambda^5} \frac{1}{exp^{(\frac{hc}{\lambda KT})}-1} d\lambda \qquad \text{Eq. (25)}$$

where F is the blackbody spectral irradiance, c is light speed ($2.9979 \times 10^8 m/s$), h is the Planck constant ($6.6238 \times 10^{-34} J.s$), K is Boltzmann constant ($1.3802 \times 10^{-23} J/K$) and T is the blackbody temperature in Kelvin. The integral of this function by the wavelength band of each filter gives the input power through filters. However, due to limited time this method could not be attempted.

The findings show that at the wavelength of 471 nm, the power conversion efficiency of the crystalline silicon solar cell is higher than the amorphous silicon solar cell. However, at 514.5 nm

the measurement result is somewhat surprising as it indicates that the amorphous silicon solar cell works more efficiently than the crystalline silicon solar cell. This contradictory result may be considered as a measurement error. At long wavelengths, the measurement result shows that the amorphous silicon solar cell works slightly more efficient at 731 nm. However, at 880 nm the crystalline silicon solar cell records a greater efficiency than that of the amorphous silicon solar cell. The result is slightly different from what was expected as the long wavelength responsivity of crystalline silicon solar cells is better than amorphous silicon solar cells. Curve fitting was applied to obtain the spectral power efficiency curve of both types of solar cells. The calculated power efficiency with respect to wavelength and the fitted curve of the spectral power efficiency of the crystalline silicon solar cell are shown in Figure 23a. Figure 23b presents the calculated power efficiency and the fitted spectral power efficiency curve as a function of wavelength of the amorphous silicon solar cell.

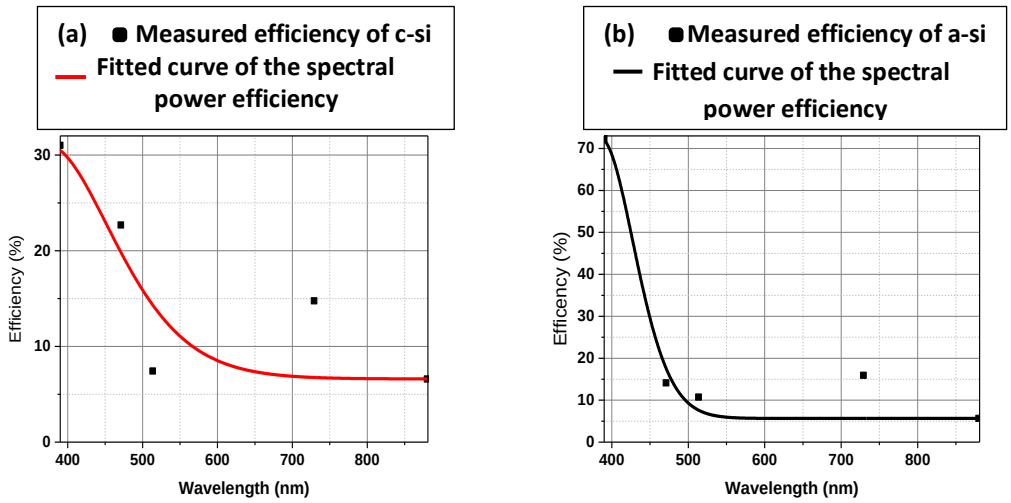

Figure 23: The calculated power efficiency (%) with respect to wavelength (nm) and the fitted curve of the spectral power efficiency of c-si and a-si.

Figure 24 displays the fitted curves of the spectral power efficiency *as* a function of wavelength of the crystalline silicon solar cell (red) and the amorphous silicon solar cell (black) plotted in one graph for comparison.

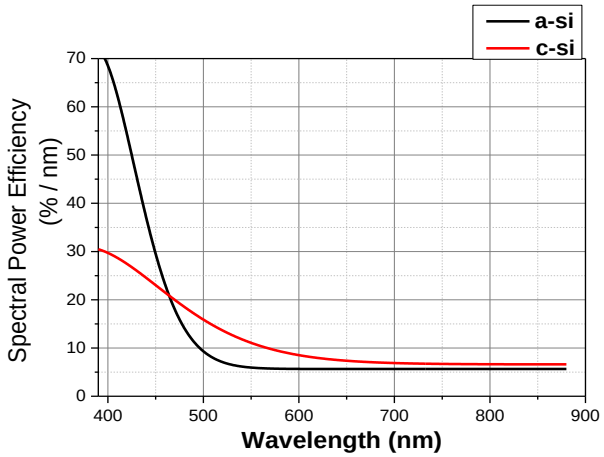

Figure 24: Approximated spectral power efficiency (%) of the crystalline and amorphous silicon solar cells.

The amorphous silicon solar cell converts high-energy photons (> 2.67 eV/ < 465 nm) into electric power with lower loss in comparison to the crystalline silicon solar cell. Since the former solar cell has a large band gap of about 1.7 eV, a high fraction of high-energy photons (> 2.67 eV/< 465 nm) could be absorbed more efficiently in comparison to the latter, i.e. crystalline silicon solar cell, which has an energy gap of about 1.1 eV. Nevertheless, the crystalline silicon solar cell produces electricity more efficiently at low-energy photons (< 2.67 eV/ > 465 nm). Although in the visible region (from 465 to 700 nm) the amorphous silicon solar cell could absorb a higher fraction of the visible light with respect to the crystalline silicon solar cell, the crystalline silicon solar cell generates electrical power more efficiently. It is possible that these results are due to the recombination mechanisms associated with amorphous silicon solar cells such as band-to-band recombination and recombination through defect states. In return, this reduces carriers' lifetime, diffusion length, and the overall efficiency of the amorphous silicon solar cell. Long wavelength photons (> 700 nm) have lower energy than the energy gap of the amorphous silicon solar cell. For example, a photon of 750 nm has an energy of 1.65 eV, and hence, it is difficult to excite an electron to the conduction band. In contrast, such photons can be highly absorbed by a crystalline silicon solar cell since its energy is higher than the energy gap. Therefore, the amorphous silicon solar cell gives lower efficiency in the near infrared region (> 700 nm) due to the large energy gap.

5 Conclusions and Future Work

The study was set out to examine the efficiency of an integrated amorphous silicon solar cell in comparison to an integrated crystalline silicon solar cell. The spectral power efficiency of both solar cells with respect to different wavelength bands of ultraviolet, visible, and near infrared regions of the solar spectrum was analysed. The study also sought to determine whether the energy gap or recombination mechanisms result in different spectral power efficiencies between the two types of silicon solar cells. The background literature regarding solar cell operation, efficiency degradation, and amorphous silicon solar cells were also detailed.

Current-voltage measurements were conducted to determine the efficiency of a crystalline silicon solar cell with an area of 1.77 mm^2 and an amorphous silicon solar cell with an area of 35 mm^2 by using a digital Picoammeter. Solar cells were illuminated by a solar simulator that gave a solar spectrum, which closely matches the Standard Extraterrestrial Spectrum AM0. Firstly, the efficiency of solar cells was measured over the entire solar spectrum AM0. The maximum power generated from solar cells was estimated as the knee point of the I-V curve. This is equivalent to the maximum generated current times the maximum voltage. The input power of the solar simulator was measured by a sun meter. The efficiency of the integrated solar cells of crystalline silicon and amorphous silicon, was hence, calculated as the maximum generated power divided by the input power of the entire solar spectrum AM0 (1 sun) over the solar cells surface area. Secondly, the efficiency of both types of solar cells were analysed against the solar spectrum wavelength to identify the spectral power efficiency of both solar cells. Each solar cell was illuminated by different wavelength bands using five filters: FB390, FB470, L-514.5, 7FB30 and FB880-40. Hence, current-voltage measurements were carried out five times for each solar cell. To calculate the efficiency of both solar cells illuminated by different wavelength bands, the maximum electrical output power and the input power of light through filters were estimated. The maximum output power was estimated from I-V curve as it is the knee point of the current-voltage curve. The input power through each filter was calculated as the ratio between the area under the filter transmission curve to the total area under the solar spectral irradiance curve AM0 (from 200-2500 nm).

The study showed that the integrated crystalline and amorphous silicon solar cells recorded an efficiency of about 5.210% and 0.293%, respectively. It is clear that the former solar cell is much more efficient than the latter. Generally, this result has confirmed the findings of the literature, which indicates that the performance of crystalline silicon solar cells is much higher than amorphous silicon solar cells.

The results of the spectral power efficiency analysis can be explained for the different regions of the electromagnetic spectrum. At short wavelengths (up to 465 nm), the amorphous silicon solar

cell gave a higher efficiency. This is because it is able to convert short wavelengths into electrical power more efficiently due to its large band gap. However, at all other wavelengths (> 465 nm), the efficiency of the crystalline silicon solar cell was higher. In the visible light region, the amorphous silicon solar cell is highly affected by recombination mechanisms; due to the direct band gap, band-to-band recombination is highly dominant. Also, defects resulting from dangling bonds increase the possibility of recombination through defect states. Together, these recombination mechanisms led to the reduction of minority carriers lifetime, the diffusion length, and hence, the reduced efficiency of the amorphous silicon solar cell. Whilst in the near infrared region, photons do not have enough of the right amount of energy to excite electrons into the conduction band, since their energy is lower than the energy gap of the amorphous silicon solar cell. Thus, the energy gap of the amorphous silicon causes a reduction in the power conversion efficiency in the near infrared region of the solar spectrum.

There are two limitations to these findings, which are acknowledged. Firstly, the spectral power efficiency of both solar cells was analysed using only five filters. Therefore, the fitted curve tool of the power conversion efficiency as a function of wavelength may not plot an accurate curve. Secondly, the solar power input through these filters is based on an assumption. It was assumed that the solar power of the wavelengths lower than 200 nm and higher than 2500 nm is absent. In addition, to find out the input power of filters, the areas under the transmission curve of filter were calculated using a simple and traditional way (divided the area to small squares and sum these squares). Consequently, the estimated input power through filters might give a slightly higher value than expected. In spite of these limitations, the findings of this dissertation add noteworthy contributions to literature on the spectral power efficiency of amorphous silicon solar cells.

Finally, further research is required to investigate closely the efficiency of the amorphous silicon solar cell, especially in the visible light. This is because, interestingly, at visible wavelengths of 400 to 465nm, the efficiency of the amorphous silicon solar cell was higher than the crystalline silicon solar cell. It would be interesting to examine whether the efficiency of both solar cells at a wavelength of 465 nm is equal or not. Further research is required to compare the minority carriers lifetime resulting from visible light in both types of solar cells. Furthermore, it would be worthwhile to investigate and solve the equation of the solar spectrum AM0, to determine a more accurate input power through filters.

6 References

Altermatt, P. P., Schmidt, J., Heiser, G., & Aberle, A. G. (1997) 'Assessment and parameterisation of Coulomb-enhanced Auger recombination coefficients in lowly injected crystalline silicon', *Journal of Applied Physics,* 82(10), p.4938-4944.

Antonini, A., Stefancich, M., Vincenzi, D., Malagú, C., Bizzi, F., A. Ronzoni, G. Martinelli Ronzoni, A., and Martinelli, G. (2003) 'Contact grid optimization methodology for front contact concentration solar cells', *Solar Energy Materials & Solar Cells*, 80, p.155–166

Araújo, G. L., and Martí, A. (1994) 'Absolute limiting efficiencies for photovoltaic energy conversion', *Solar Energy Materials and Solar Cells,* 33(2), p.213-240.

Bhattacharya, J. (2013) *Understanding the physics of degradation of polymer solar cell.* PhD. Iowa State University.

Boutchich, M., Alvarez, J., Diouf, D., Roca, I., Cabarrocas, P., Liao, M., Masataka, I., Koyadi, Y. & Kleider, J. P. (2012) *'Amorphous silicon diamond based heterojunctions with high rectification ratio'*, Journal of Non-Crystalline Solids, 358(17), p. 2110-2113.

Böer, K. W. (2013) 'Amorphous Silicon Solar Cells', In: *Handbook of the Physics of Thin-Film Solar Cells*, Springer-Verlag Berlin Heidelberg, p. 721-738. ISBN: 978-3-642-36747-2 [Print] 978-3-642-36748-9 [Online].

Carson, J. A. (2008) *'Solar Cell Research Progress'*. Nova Science Publishers, Inc. New York.

Castañer, L and Silvestre, S. (2002) Modelling Photovoltaic Systems Using Pspice, John Wiley & Sons, Chichester.

Dadu M., Kapoor, A., and Tripathi, K. A. (2002) 'Effect of operating current dependent series resistance on the fill factor of a solar cell', *Solar Energy Materials a Solar Cells,* 71, p. 213–218.

Deng, X. and Schiff, E. S. (2003) 'Amorphous Silicon–based Solar Cells', In: Luque, A. and Hegedus, S. *Handbook of Photovoltaic Science and Engineering*. John Wiley & Sons, Ltd ISBN: 0-471-49196-9.P.506-565.

DIRECTIVE OF THE EUROPEAN PARLIAMENT AND OF THE COUNCIL ON THE PROMOSION OF THE USE OF ENERGY FROM RENEWABLE SOURCES (2008) COMMISSION OF THE EUROPEAN COMMUNITIES, Brussels, 23/01/2008. Available at: http://ec.europa.eu/energy/climate_actions/doc/2008_res_working_document_en.pdf (Accessed 28 June 2014).

Dyk, E.E. and Meyer, E.L. (2004) 'Analysis of the effect of parasitic resistances on the performance of photovoltaic modules', *Renewable Energy,* 29, p. 333–344.

Emery, K. (2003) 'Measurement and characterization of solar cells and modules', *Handbook of Photovoltaic Science and Engineering,* 1, p. 701-752.

Emery, K., & Moriarty, T. (2008) 'Accurate measurement of organic solar cell efficiency', In: *Photonic Devices+ Applications.* International Society for Optics and Photonics, 1617 Cole Blvd., Golden, CO 80401, USA, in August 2003, p. 70520D1-70520D6.

FÖll, H. (2011) 'Characteristics of Real Solar Cell': Semiconductor Technology. [Online] Available at: http://www.tf.uni-kiel.de/matwis/amat/semitech_en/index.html (Accessed 2 July 2014).

Fonash, S. (2010) 'Solar Cell Device Physics', 2nd edition. New York: Academic Press.

Fritzsche, H. (2001) 'Development in understanding and controlling the Staebler-Wronski effect in a-Si: H', *Annual Review of Materials Research*, 31(1), p.47-79.

Fujioka, Y., Shimizu, A., Fukuda, H., Oouchida, T., Tachibana, S., Tanamura, H., Nomoto, K., Okamoto, K., & Abe, M. (2006) 'Large-scale, high-efficiency thin-film silicon solar cells fabricated by short-pulsed plasma CVD method', *Solar energy materials and solar cells,* 90(18), p. 3416-3421.

García-Tabarés, E., & Rey-Stolle, I. (2014) 'Impact of metal-organic vapor phase epitaxy environment on silicon bulk lifetime for III–V-on-Si multijunction solar cells', *Solar Energy Materials and Solar Cells*, 124, p.17-23.

Gottschalg, R., Betts, T. R., Infield, D. G., & Kearney, M. J. (2005) 'The effect of spectral variations on the performance parameters of single and double junction amorphous silicon solar cells', *Solar energy materials and solar cells*, *85* (3), p. 415-428.

Green Rhino Energy (2014) The Principles of Photovoltaics. [Online] Available at: http://www.greenrhinoenergy.com/solar/technologies/pv_cells.php (Accessed 29 July 2014).

Guha, S., Yang, J., and Banerjee, A. (2000) 'Amorphous Silicon Alloy Photovoltaic Research Present and Future', *PROGRESS IN PHOTOVOLTAICS: RESEARCH AND APPLICATIONS*, 8, p. 141–150.

Haberlin, *N. (2012) 'Photovoltaics System Design and Practice': Translated By Herbert Eppel:* John Wiley & Sons Inc., eISBN-13: 9781119977001 eISBN-10: 1119977002 Print ISBNs: HB: 9781119992851, 1119992850.

HAMAMATSU, Photodiode technical information. [Online] Available at: http://people.na.infn.it/~garufi/didattica/CorsoAcq/Trasp/Lezione3/photodiode_technical_information.pdf (Accessed 16 July 2014).

Hegedus, S. S. and Shafarman, W. N. (2004) 'Thin-Film Solar Cells: Device Measurements and Analysis', *PROGRESS IN PHOTOVOLTAICS: RESEARCH AND APPLICATIONS,* 12, p.155–176.

Hernday, P. (2011) '*Field Applications for I-V Curve Tracers'.* [Online] Available at: http://solarprofessional.com/articles/design-installation/field-applications-for-i-v-curve-tracers (Accessed 11 July 2014).

Huang, J. Y., Chien Y. L., Chang-Hong, S., Jia-Min, S., and Bau-Tong, D. (2012) 'Low cost high-efficiency amorphous silicon solar cells with improved light-soaking stability', *Solar Energy Materials & Solar Cells,* 98, p. 277-282.

Julian Chen, C. (2011) *'Physics of Solar Energy'*: John Wiley & Sons Inc., eISBN-13: 9781118044575 eISBN-10: 1118044576 Print ISBNs: HB: 9780470647806, 0470647809.

KEITHLEY Instrument Application Note Series (2000) Making I‑V and C‑V Measurements on Solar/Photovoltaic Cells Using the Model 4200‑SCS Semiconductor Characterization System. [Online] Available at: www.keithley.co.uk/data?asset=50913 (Accessed 11 July 2014).

Kitai, A. (2011) '*Principles of Solar Cells, LEDs and Diodes: the role of the PN junction*', United Kingdom: John Wiley & Sons.

Liu, B. (2014) 'Light management in hydrogenated amorphous silicon germanium solar cells', *Solar Energy Materials & Solar Cells,*128, p. 1-10.

Ludowise, M. and Frass, L. (2010) 'High-Concentration Cassegrainian Solar Cell Modules and Arrays', In: Fraas, L. M. and Partain, L. D. (2nd edition) *Solar Cells and Their Applications, Wiley Series in Microwave and Optical Engineering*. New Jersey: John Wiley & Sons, Inc. p.337-358.

Mah, O. (1998) 'Fundamentals of photovoltaic materials', *National Solar Power Research Institute,* Inc. [Online] Available at: http://userwww.sfsu.edu/ciotola/solar/pv.pdf

Markvarta, T., & Castañerb, L. (2011) 'Principles of solar cell operation', *Practical Handbook of Photovoltaics: Fundamentals and Applications*, 7, Elsevier Ltd.

McMahon, T.J., Basso, T.S., and Rummel, S.R. (1996) 'Cell shunt resistance and photovoltaic module performance', In: *Proceedings of the 25th Photovoltaic Specialists Conference*, p. 1291–1294.

Nagle, T. J. (2007) *Quantum efficiency as a device-physics interpretation tool for thin-film solar cells* ProQuest. PhD. Colorado State University.

Nann, S., & Emery, K. (1992) 'Spectral effects on PV-device rating', *Solar Energy Materials and Solar Cells*, *27* (3), p. 189-216.

Nelson, J. (2003) *'The physics of solar cells'* (Vol. 57). London: Imperial college press.

Newport corporation, Introduction to Solar Radiation. [Online] Available at: http://www.newport.com/Introduction-to-Solar-Radiation/411919/1033/content.aspx (Accessed 28 Augest 2014)

NREL Renewable Resource Data Centre (2014) ASTM Standard Extraterrestrial Spectrum Reference E-490-00. Available at: http://rredc.nrel.gov/solar/spectra/am0/ (Accessed: 11 July 2014).

Photovoltaic Education (2014) Quantum Efficiency. [Online] Available at: http://pveducation.org/pvcdrom/solar-cell-operation/quantum-efficiency (Accessed 1 July 2014).

Photovoltaic Education (2014) Semiconductor Materials. [Online] Available at: http://www.pveducation.org/pvcdrom/pn-junction/semiconductor-materials (Accessed 28 June 2014).

Photovoltaic Education (2014) Spectral Response. [Online] Available at: http://pveducation.org/pvcdrom/characterisation/spectral-response (Accessed 1 July 2014).

Prajapati, V. (2013) *'Advanced Front Side Technology on Crystalline Silicon Solar Cell'*, PhD, In collaboration with imec. ISBN 9460186408, 9789460186400.

Pysch, D., Mette, A., and Glunz, S.W. (2007) 'A review and comparison of different methods to determine the series resistance of solar cells', *Solar Energy Materials & Solar Cells*, 91, p. 1698–1706.

Qin, Y., Yan, H., Li, F., Qiao, L., Liu, Q., and He, D. (2010) 'The optoelectronic properties of silicon films deposited by inductively coupled plasma CVD', *Applied Surface Science,* 257, p. 817–822.

Radue, C. and Dyk, E. E., (2010) 'A comparison of degradation in three amorphous silicon PV module technologies', *Solar Energy Materials & Solar Cells,* 94, p.617–622.

Rahman, M. Z. (2012) 'Modeling Minority Carrier's Recombination Lifetime of p-Si Solar Cell', *INTERNATIONAL JOURNAL OF RENEWABLE ENERGY RESEARCH*, 2 (1), p.117-122.

Rech, B. and Wagner, H. (1999) 'Potential of amorphous silicon for solar cells', *Applied Physics A Materials Science & Processing*, 69, p. 155–167.

Rein, S. (2006) 'Lifetime spectroscopy: A method of defect characterization in silicon for photovoltaic applications', (Vol. 85). Springer.

Rhys, J. (2011) *'Cumulative Carbon Emissions and Climate Change: Has the Economics of Climate Policies Lost Contact with the Physics',* [Online] Available at: http://www.oxfordenergy.org/wpcms/wp-content/uploads/2011/07/EV-571.pdf (Accessed 25 June 2014).

Saga, T. (2010) 'Advances in crystalline silicon solar cell technology for industrial mass production', *NPG Asia Materials,* 2(3), p. 96-102. [Online] Available at: http://www.nature.com/am/journal/v2/n3/full/am201082a.html (Accessed 17 Sep 2014).

SANYO (2007) *'Amorphous Silicon Solar Cell/ Amorphous Photosensor',* [Online] Available at: http://us.sanyo.com/Dynamic/customPages/docs/solarPower_Amorphous_PV_Product_Brochure%20_EP120B.pdf (Accessed 28 July 2014).

Sheng, S. L. (2007) '*Semiconductor Physical Electronics*'. New York: Springer Science & Business Media.

Smets, A. H. M., Matsui, T., & Kondo, M. (2008) 'High-rate deposition of microcrystalline silicon pin solar cells in the high pressure depletion regime', *Journal of applied physics,* 104(3), p. 034508.

Soffer, B. H. and Lynch, D. K. (1999) 'Some paradoxes, errors, and resolutions concerning the spectral optimization of human vision', *American Association of Physics Teachers,* 67 (11), p. 946- 953. Available at: http://www.phys.ufl.edu/~hagen/phz4710/readings/AJPSofferLynch.pdf

Solanki, C. S. (2009) *'Solar Photovoltaics: Fundamentals Technologies And Applications'. New Delhi:* PHI Learning Private Ltd., ISBN8120337603, 9788120337602.

Strümpel, C., McCann, M., Beaucarne, G., Arkhipov, V., Slaoui, A., Švrček, V., Del Cañizo, C., and Tobiaset, I. (2007) 'Modifying the solar spectrum to enhance silicon solar cell efficiency_ An overview of available materials', *Solar Energy Materials & Solar Cells, 91, p. 238–249.*

Sun, G. (2010) 'The Intersubband Approach to Si-based Lasers', In: Costa, N. and Cartaxo, A. (eds.), *Advances in Lasers and Electro Optics.* InTech, p. 255-289. ISBN 978-953-307-088-9

Takatsuka, H., Noda, M., Yonekura, Y., Takeuchi, Y., and Yamauchi, Y. (2004) 'Development of high efficiency large area silicon thin film modules using VHF-PECVD', *Solar Energy*, 77(6), p. 951-960.

Tao, M. (2014) 'Physics of Solar Cells', In: *Terawatt Solar Photovoltaics*. London: Springer Briefs in Applied Science and Technology, p.21-45.

TFI TECHNOLOGIES Thin Film Imaging (2014) Laserline L-514.5-10. [Online] Available at: http://www.tfitech.com/servlet/the-Laserline-dsh-1,3,10-FWHM/Categories (Accessed: 10 July 2014).

The Renewable Energy Directive, (2008) [Online] Available at: http://www.ewea.org/fileadmin/ewea_documents/documents/00_POLICY_document/RES_Directive_special.pdf (Accessed 25 June 2014).

The Office of Energy Efficiency and Renewable Energy (EERE), Amorphous silicon. [Online] Available at: http://energy.gov/eere/sunshot/amorphous-silicon (Accessed 18 Sep 2014).

THE UNITED NATIONS FRAMEWORK CONVENTION ON CLIMATE CHANGE (1998) KYOTO PROTOCOL. [Online] Available at: http://unfccc.int/resource/docs/convkp/kpeng.pdf (Accessed: 28 June 2014).

THORLABS (2014) Band pass & Laser Line Filters. [Online] Available at: http://www.thorlabs.de/navigation.cfm?guide_id=2210 (Accessed: 10 July 2014).

Trupke, T., Green, M. A., and Würfel, P. (2002) 'Improving solar cell efficiencies by down-conversion', *Journal Of Applied Physics, 92(3), p.1668-1674.*

Tyagi, V. V., Rahim, N. A., Rahim, N. A., and Selvaraj, J. A. (2013) 'Progress in solar PV technology: research and achievement', *Renewable and sustainable energy reviews,* 20, p. 443-461.

Vetterl, O., Finger, F., Carius, R., Hapke, P., Houben, L., Kluth, O., Lambertz, A., Mück, A., B. Rech, B. and Wagner, H. (2000) 'Intrinsic microcrystalline silicon: A new material for photovoltaics', *Solar Energy Materials and Solar Cells,* 62 (1), p. 97-108.

Wagner, S., Carlson, D. E., and Branz, H. M. (1999) 'Amorphous and microcrystalline silicon solar cells', In Photovoltaics for *the 21st Century: Proceedings of the International Symposium.* The Electrochemical Society, Seattle, Washington 99 (11), p. 219.

Willis, S. (2011) *Advanced optoelectronic characterisation of solar cells.* PhD. Oxford University.

Wronski, C. R., and Carlson, D. E. (2001) 'Amorphous silicon solar cells'. *Clean Electricity from Photovoltaic, Imperial College Press*, UK, p. 99-244.

Würfel, P. and Würfel, U. (2009) 'Physics of Solar Cells: From Basic Principles to Advanced Concepts', John Wiley & Sons Inc.

Zeman, M. (2006) 'Solar Cell Operational Principles', In: Solar Cells. *Delft University of Technology*.

Zhou, W., Yang, H., and Fang, Z. (2007) 'A novel model for photovoltaic array performance prediction', *Applied Energy,* 84 (12), p.1187–1198.

7 Appendix

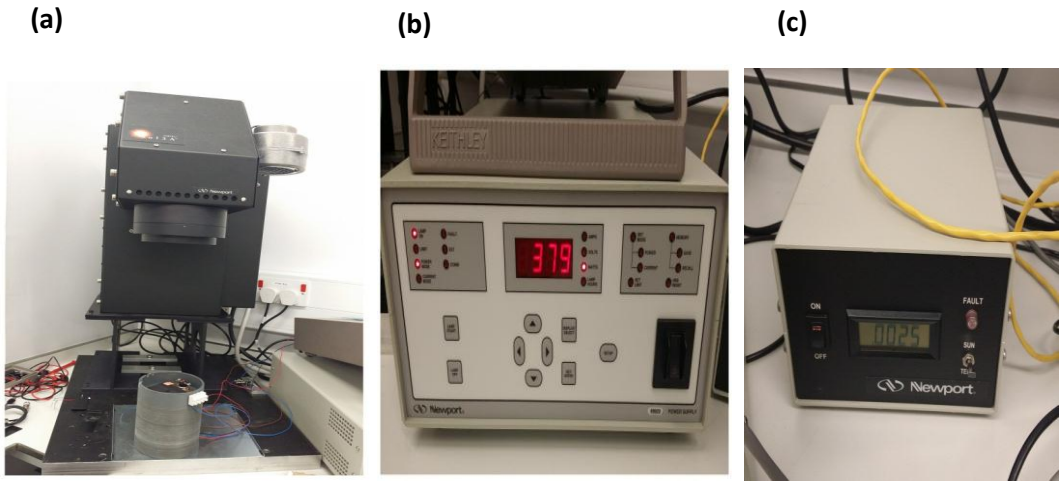

Figure 1: Sol3A ORIEL (Newport) solar simulator package used in the current *versus* voltage measurement.

(a) Solar simulator source for illuminating solar cells. (b) Power source of the solar simulator device. (c) Sun/temperature meter used to measure the solar irradiation of the solar simulator.

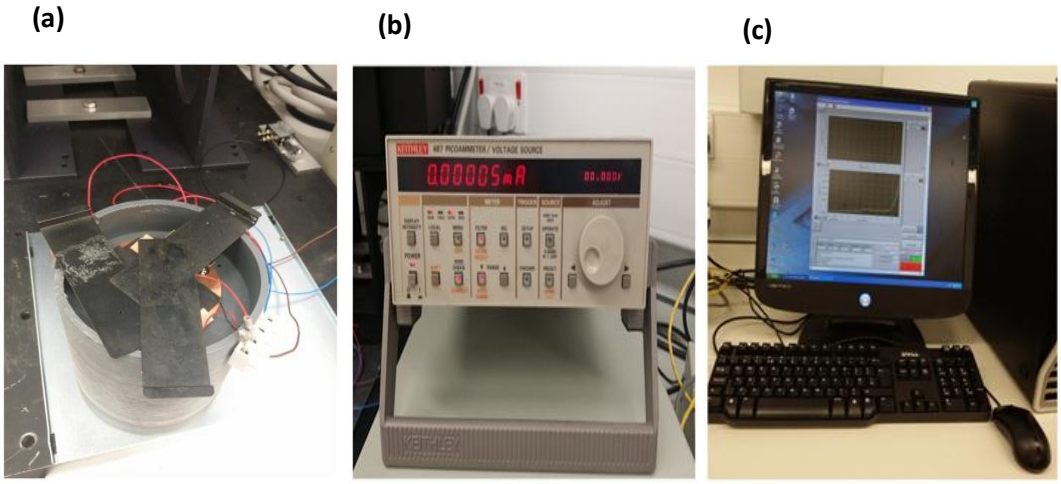

Figure 2: Current *versus* voltage measurement procedures.

(a) A mask with a hole used on the top of solar cells to determine a sample area and then placed on a holder to be illuminated by the solar simulator. (b) Picoammeter (KEITHLEY) used to measure the photocurrent with respect to bias voltage. (c) Lab view connected to the Picoammeter where the current-voltage curve is plotted.

Figure 3: Five filters used to analyse the power conversion efficiency of solar cells in ultraviolet, visible, and near infrared region of the solar spectrum.

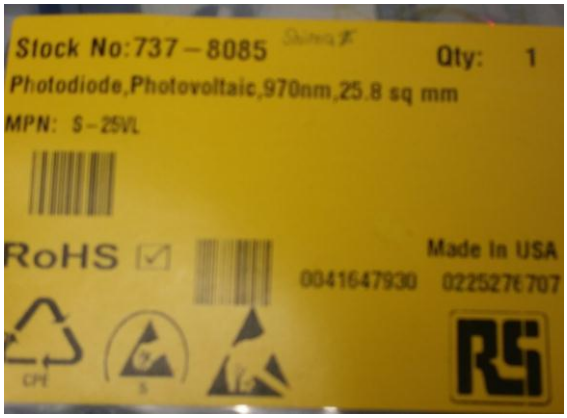

Figure 4: The photodiode data that used as a standard crystalline silicon solar cell.

ANALYSIS OF THE INTEGRATED AND SPECTRAL POWER EFFICIENCY OF THE AMORPHOUS PV CELL

EEEN60198 Feasibility Study 2013-14 2nd Semester

Renewable Energy and Clean Technology Program

Nouf Saad Alkathran

8519212

Supervised by:

Prof. Bruce Hamilton

Submitted on 14 July 2014

Abstract

Nowadays, solar energy is one of clean energy resources that is receiving an increasing interest by engineers and researchers. Improve and analyse the efficiency of photovoltaic cells are the aim of many studies. This research project is set to examine the efficiency of amorphous silicon solar cell against crystalline silicon solar cell and to analyse the causes of the differences. This will be completed by performing a current versus voltage measurement experiment and then the efficiency will be calculated. The corresponding quantum-efficiency spectra for amorphous silicon and crystalline silicon solar cells will be plotted. A solar simulator and HP Picoammeter will be employed to obtain the measurements. Filters will be also used in order to get data for different spectrum. The measured data will then be analysed to obtain conclusions on the efficiency of amorphous silicon cell. A risk assessment has been carried out to identify any expected hindrances for the project and a risk mitigation plan is set. Project tasks and time schedule have been developed to insure on time completion of the project. The results of this research will be beneficial for manufacture as it identify the potential area for improving the efficiency of amorphous silicon cell.

Table of Contents

1 Introduction

The need for obtainable and clean energy has led to more remarkable improvements in sustainable energy sources. Exploiting solar energy by photovoltaic technologies is a promising and interesting source. The performance of PV devices has been assessed according to different parameters (Nann and Emery, 1992). The peak power output of the PV devices is the most essential indicator to evaluate their efficiency.This is because the price of PV systems is considered according to the power generated.

Historically, classical semiconductors such as mono and multi crystalline silicon were the most devices attracted researchers attention. The maximum measured efficiency of the mono silicon is 15% to 25% (Green et al., 2010).Their optimum efficiency is quite low compared to the high cost of manufacturing processes. Such manufacturing processes require high temperature, which in turn leads to emit more CO_2 to the atmosphere. Owing to these weaknesses on the performance of the classical devices, research interest has shifted toward alternative materials. Alternative devices such as amorphous silicon cell have been developed. These devices are cheaper and easier to manufacture than mono silicon crystalline. The main feature of amorphous silicon cells is that it can be made as a thin film which results in saving silicon material. Moreover, the manufacturing processes of amorphous silicon do not require high temperature so that it can be deposited on different substrates such as metal, glass and plastic (Böer, 2013). These reasons and other physics related reasons make amorphous silicon a promising alternative for solar cells. Hence, research and experiments about the performance of amorphous silicon solar cells are worthwhile.

1.1 Background

Photovoltaic cells (PV) are presented as p-n junction (diode). The p and n layers are semiconductor cells, e.g., silicon, doped by donor or acceptor atoms to enhance their conductivity (σ). Donor impurity is achieved when Phosphorus (P) atoms (5 outer electrons) donate electrons to the conduction band of the semiconductor cell. In this case the semiconductor is called n-type. While Acceptor impurity is obtained when Boron (B) atoms replace silicon atoms, which leads to create holes in the valence band of the semiconductor, and hence, change their conductivity. This type of a semiconductor is known as p-type. Putting n and p types in contact leads to electrons transferring from n-type to p-type (diffusion). These electrons recombine with holes created in the p-type. Consequently, this creates positive ionised charges in the n-type and negative ionised charges in the p-type. The transferring of electrons continues until equilibrium is reached. The equilibrium is achieved when the minority electron in p-type is equal to the majority electrons in

the n-type. The negative and positive charges create a depletion region near the junction. Potential barrier is then created, which prevents majority carriers of crossing the p-n junction whereas minority carriers are collected as photocurrent (Haberlin, 2012).

Originally, PV cells generate current in reverse direction by optical absorption processes. Exposure PV cells into sunlight results in absorbing some photons (ph). Absorbing photons near the depletion region excites electrons from the valence band to conductor band creating minority carriers electrons and holes in the p and n layers, respectively. These minority carriers, resulting from photons absorption, are captured by the electric field of the depletion region. Hence, photo-induced current is generated in the reverse bias. The amount of this current depends on the density of the minority carriers enhanced by light absorption (Julian Chen, 2011).

To extract power from the diode, a load resistor (R) must be added. The equivalent diode photocurrent circuit is presented in Figure (1a). As a result, forward bias voltage appears, according to voltage drop, across the resistor. Consequently, the total current flow is reduced. When the load resistor is equal to zero, short circuit current (I_{sc}) appears in the reverse direction. Increasing R leads to increase the forward bias voltage while the current flow is not affected since the current forward is very small. However, beyond a critical value of the resistor, namely R optimum, the forward current rapidly increases while the reverse current (photo current) decreases. When the resistance equals to maximum value, the photocurrent collapses to zero. Figure (1b) presents how the forward current offsets the reverse current when R increases. In order to operate the cell to extract the maximum power, namely the knee point of the curve, an optimum resistor should be applied that is equal to V_{max}/I_{max} . Another important point is that the optimum R depends on the solar density, so the value of optimum R should be varied during the day. Photocurrent influences the light intensity as well, which produces a challenge to connect solar panels into the grid system (Haberlin, 2012).

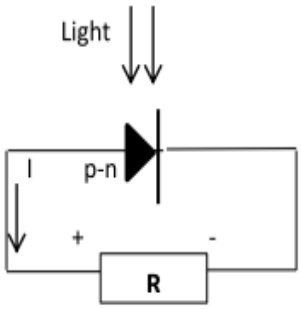

Figure (1a) Photocurrent equivalent circuit.

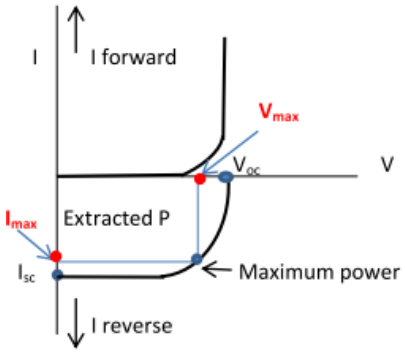

Figure (1b) Current biases vs. voltage.

The performance of solar cells is evaluated by three parameters: fill factor, efficiency, and quantum efficiency. The fill factor (FF) indicates the quality of the solar cells. It gives an idea of the performance as comparison between the solar cell and an ideal cell. The fill factor is given as the ratio between maximum power generated from the solar cell and the V_{oc}*I_{sc} that are produced (see the equation 1) (Haberlin, 2012, Tao, 2014, KEITHELY Instrument Aapplication Note Series, 2000).

$$FF = \frac{I_{mpp} \times V_{mmp}}{I_{sc} \times V_{oc}} = \frac{P_{max}}{I_{sc} \times V_{oc}} \qquad (1)$$

The practical indicator to describe the performance of a PV device is a power conversion efficiency (η). It gives the ratio between the maximum power produced (P_{max}) to the total power input. Where the power input means the total incident irradiance (E_{tot}) on the area (A) of the cell. The efficiency is estimated by the equation (2) (Julian Chen, 2011, Emery and Moriarty, 2008):

$$\eta = \frac{P_{max}}{E_{tot} \ A} \qquad (2)$$

Quantum efficiency is another key indicator for solar cell performance. External quantum efficiency (EQE) presents the relationship between the photocurrent produced by the cell and the total number of photons in the incident light. Whereas the internal quantum efficiency (IQE) takes into account all generated carriers, including losses owing to recombination or light reflection. The EQE indicator is more important than IQE (Editorial, 2008).

Most research aims to improve solar devices that give higher power with low cost. However, there are many factors, which limit the power efficiency of the solar cell. Reducing the cell losses is the essential solution weather they are due to the behaviour of the carriers or light losses (Julian Chen, 2011, Haberlin, 2012).

Solar irradiation consists of a wide range of wavelength (λ), and hence a different level of energy (E). Some photons do not have an adequate energy to excite electrons from a valence band to a conductive band. Their energy is lower than the bandgap energy of the cell (E_g). These photons pass through the cell without inducing significant effect. Other photons have energy that greater than the bandgap. This in turn causes loss in the form of thermal energy due to the penalty energy of the photons. These two problems cannot be controlled by the fabrication of single semiconductors. One solution of these issues is manufacturing solar cells with multi-junction such as Tandem cells. These kinds of cells are made of different material to have different bandgap values in order to match the solar spectrum (Julian Chen, 2011, Haberlin, 2012, Tao, 2014).

Other issue is that not the entire incident light enters the cells; some light reflects from the surface of the cell. To limit light loss, antireflection coating (ARC) is applied to the cells surface. Additionally, texture surface is applied to trap light which lower the light loss (Julian Chen, 2011, Haberlin, 2012).

In addition, the finite thickness of a cell influences the power conversion efficiency considerably. Owing to the limited thickness of the absorber layer determined by absorption coefficient (α), the absorption of incident light could be incomplete. This issue is more significant for indirect gab cells such as silicon (Si) and germanium (Ge) because the length of the extinction depth (1/α) is long. In other word, the absorption coefficients (α) of them are low. In contrast, the optical absorption coefficient of amorphous silicon cells is high as it is classified as direct bandgap semiconductors. However, the problem of incomplete absorption can be fixed by designing back face reflection for the cells in order to return the photons into the absorption layer again (Haberlin, 2012).

Moreover, the shading loss due to the metal electrode coverage is a source of reducing the power conversion efficiency. The metal coverage reduces the transparent area, and hence, the amount of light entering the cell reduces. A grid pattern is optimally designed to control both shading and series resistance losses resulting from the front contact of the cell (Tao, 2014).

Carriers charge behaviour is the main reason for decreasing the cell efficiency due to the recombination mechanism. The recombination issue occurs because of the deep level
(defect state) located in the bandgap where excited carrier can be captured before reaching the conduction band. Such deep level might be created due to transition metal contamination during cell manufacturing. The effect of the deep level for silicon cells could be mitigated by coating the cell with Silicon Nitride (SiNx:H). Recombination could also happen at the front and the back surfaces of the cells, which adds more losses (Tao, 2014). For the silicon cell, for example, back face recombination may be reduced by coating a thin layer of acceptor impurity such as (Al).

When the coating is heated up, Al atoms ionise the p-type changing it to p^+. This produces an energy band, which prevents minority carriers from reaching the back surface and reflects them to the active region (the depletion layer).

The efficiency value of solar cells depends on the fill factor value as the efficiency (η) is defined as:

$$\eta = \frac{I_{sc} \times V_{oc}}{P_{in}} \times FF \qquad (3)$$

Having high fill factor improves the efficiency of the cell (Haberlin, 2012). The fill factor, however, is influenced by series resistance (R_s). The high value of series resistance reduces the fill factor as it is described in the following equation:

$$FF \approx FF_0 \, (1 - r_s \,) \qquad (4)$$

Where FF_0 is the fill factor with zero series resistance and (r_s) is the series resistance given by:

$$r_s = R_s \, \frac{I_{sc}}{V_{oc}} \qquad (5)$$

Series resistance plays an essential role in controlling the cell performance. Increase series resistance reduces the current (J) and the maximum power extracted from the cell. This in turn limits the efficiency of the cell. For example, series resistance of 10 Ohm damages the cell. Figure (2.a) shows the impact of different values of series resistance (R_s) with constant shunt resistance (R_{sh}) on the cell performance. Series resistance (R_s) is determined by several factors such as: the resistance of the metal top contact, emitter, fingers of the top grid, junction depth, and ohmic losses. Another resistance associated with solar cells is the shunt resistance (R_{sh}), also known as the parallel resistance (R_p). Shunt resistance is created due to a deep level state in the depletion layer and cell defects. When the shunt resistance increases, the cell performance will be more optimal. Generally, its issues are less problematic than those of the series resistance. Figure (2.b) presents the effects of different values of shunt resistance with constant series resistance (FÖll, 2011).

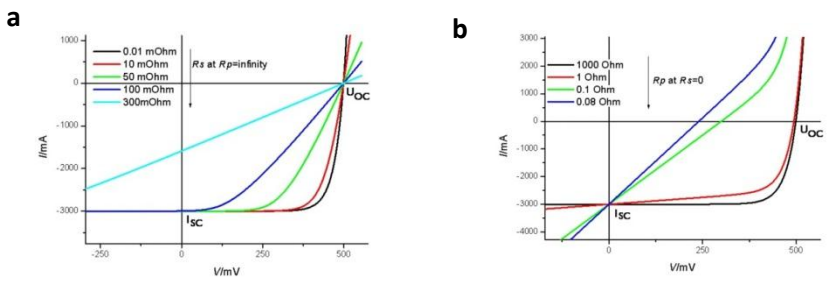

Figure (2a) The effect of series resistance and (2b) shunt resistance on the cell performance (FÖll, 2011).

The real non- ideal solar cell equivalent circuit is presented in the figure (3) (Haberlin, 2012, Tao, 2014, FÖll, 2011). The total current for the real PV cell connecting to a load resistor is given by:

$$J = J_{ph} - J_s\{\exp\left[\frac{q(V+JR_s)}{nkT}\right] - \frac{V+J\,R_s}{R_{sh}} \qquad (6)$$

Where: J_s is the saturation current and J_{ph} is the photocurrent

Ideally, to reduce the loss due to the resistances, the value of series resistance should be 0 while for shunt resistances should be infinite. The ideal value of the (n) factor is 1 to 2.

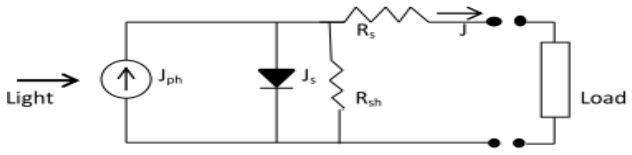

Figure (3) The real PV equivalent circuit.

To minimise the effect of series resistance, some fabrication aspects are introduced such as n-type for the top contact layer, thick top contact (emitter): but depletion layer should be close to the surface to collect carrier more efficiently, transparently of the top contact, and optimal doping (Tao, 2014).

1.2 Main aim and objectives

In the light of all this, this project aims to measure the efficiency of an amorphous silicon cell by using a solar simulator. Differences between a standard silicon cell (c-si) and an amorphous silicon cell (a-si) will be identified. Physical and electrical properties of (a-si) will be investigated to determine the reasons of having different losses from those of (c-si).

To accomplish the aim of this project the following objectives have to be completed:

- Conducting critical literature review on the efficiency measurement of a calibrated silicon cell and an amorphous silicon cell by using a solar simulator.
- Designing an experiment for I-V characteristic measurement of a calibrated silicon cell and an amorphous silicon cell by using a solar simulator.
- Analysing recorded data and calculating the efficiency using equation 2.
- Plotting two graphs; the current -voltage curve and efficiency versus spectrum energy graph for both the silicon cell and the amorphous silicon cell.
- Discussing the result to obtain a conclusion on the efficiency of the amorphous silicon cell with respect to the silicon cell.
- Writing the final report.

2 Literature Review

2.1 Current-Voltage Measurement of PV Cells

2.1.1 Solar Simulator

Solar simulator is a light source used in labs for efficiency measurement of PV cells. It gives solar spectrum similar to sunlight which can be a standard source used in labs to assess the performance of solar cells. The perfect solar source must give less than ±1% difference in the light level when the current and voltage of PV cells are measured. Additionally, the maximum mismatch error in the spectral between the reference cell, usually crystalline silicon, and test cells introduced by the perfect solar simulator should be less than 1%. These above conditions are reduced the uncertainty level of efficiency calculation to less than ±2% (Emery, 2003).

The illumination sources of typical solar simulators are continuous arc, pulsed arc, and filament lamps. The efficiency measurement could be reduced due to light reflection when the test cell is placed very near to the optical source. This type of reflection is known as reflection-related artifact, which exists as a result of the mismatch of the field of view of the reference cell and test cell. The reflection-related artifacts also could happen due to reflections off the light source, calibrated reference cell, the test cell capsulate and the area under the test cell. The light reflection because of the area under the test cell is particularly critical for double-sided cells (Emery, 2003).

2.1.2 Spectral Mismatch Error

All efficiency measurement of PV cells encounters a spectral error. The correction factor of the spectral error is calculated by (Emery and Moriarty, 2008, Emery and Osterwald, 1989, Emery et al., 1985):

$$M = \frac{\int_{\lambda_1}^{\lambda_2} E_{Ref}(\lambda)\, S_R(\lambda)\, d\lambda \int_{\lambda_1}^{\lambda_2} E_S(\lambda) S_T(\lambda) d\lambda}{\int_{\lambda_1}^{\lambda_2} E_{Ref}(\lambda)\, S_T(\lambda)\, d\lambda \int_{\lambda_1}^{\lambda_2} E_S(\lambda) S_R(\lambda)\, d\lambda} \qquad (7)$$

where E_{Ref} indicates the solar spectral irradiance , E_s is the spectral irradiance of the light source, S_R is the spectral responsivity of the reference cell and S_T is the spectral responsivity of the test cell , all these parameters are function of wavelength (λ).

For efficiency measurement using a solar simulator, the current- voltage values are obtained at a correct light level. This is achieved by dividing the reference cell calibration value by M rather than changing the measured current for M to the right value. Then the light source is attuned in order to make the short circuit current of the reference cell and their spectrally corrected calibration values identical. To increase the probability of having M equals to one, the best scenario is to use

a reference cell whose spectral responsivity is similar to the spectral responsivity of the test cell. Alternatively, it is better to use the light source that has spectral irradiance matches the reference spectrum. Hence, it is essential to use a matched reference cell in order to avoid the correction of M. Therefore, in testing amorphous silicon and organic cells, crystalline silicon is used as a reference cell with colour glass filter to make their spectral responsivity congruous (Emery and Moriarty, 2008, Emery, 2003).

2.1.3 Simulator-Based Calibration Procedure

The short circuit current generated from a test cell ($I^{T,R}$) measured at the reference irradiance (E_{Ref}) could be estimated by (Nann and Emery, 1992):

$$I^{T,R} = \frac{I^{T,S} E_{Ref}\, CV}{I^{R,S}\, M} \qquad (8)$$

where $I^{T,S}$ is the short-circuit current generated from a test cell gauged using the light source, M is the correction factor, CV is the calibration value, and $I^{R,S}$ is the short-circuit current generated from the reference cell gauged using the light source. Typically, it is assumed that M is equal to unity because it is difficult to have information about the spectral irradiance of the light source and the spectral responsivity of a reference cell and a test cell. Hence, the simulator is attuned to make the effective irradiance (E_{tot}) is equal to reference spectral irradiance(E_{Ref}). Generally, to make M is equal to unity, the reference and test cells are made from the same material using same technology, hence, the spectral responsivities of reference and test cells will be identical (Emery,2003).

2.2 Quantum Efficiency Measurements

Emery (2003) states that the quantum efficiency QE(λ) or spectral responsivity S(λ) is an important indicator to comprehend the different mechanisms in the PV cells such as electron-hole generation and recombination. The spectral responsivity is gauged in units of current generated per unit power. The spectral responsivity S(λ) then can be converted to minority charge carriers generated per photon entering the cell by the following equation:

$$QE(\lambda) = \frac{qS(\lambda)}{\lambda hc} \qquad (9)$$

where hc/q is 0.80655 when the unit of micrometer (μm) is used for the wavelength and ammeter per watt (A/W) for the spectral responsivity. The quantum efficiency can be calculated by multiplying the yield of the electron- hole generated per incident photon by 100.

2.3 Amorphous Silicon Solar Cell

2.3.1 The potential of Amorphous Silicon Solar Cells

Amorphous silicon is a noncrystalline semiconductor, but the chemical bonding between its atoms is similar to that of crystalline semiconductors. Nevertheless, their bonds are small and disorder, and hence the angle between their bonds is varied causing dangling bonds. The dangling bonds form defects, which in turn limit the performance of the amorphous silicon solar cells. The effect of the dangling bonds could be mitigated by hydrogen passivation where the dangling bond bonds to hydrogen (Deng and Schiff, 2003). The hydrogenated form of amorphous silicon is commonly known as hydrogenated amorphous silicon (a-si:H). Generally speaking, the term of amorphous silicon cited in many papers means the hydrogenated form.

As mentioned earlier, the absorption coefficient (α) of amorphous silicon exceeds that for crystalline silicon. This feature improves the exploiting solar energy in a thin layer since it is a direct bandgap semiconductor. Figure (4) describes the absorption coefficient (α) in the unit of (cm^{-1}) with respect to photon energy (hv) in the unit of (eV) for hydrogenated amorphous silicon cell (a-si:H) and a monocrystalline silicon cell (c-si) (Böer, 2013).

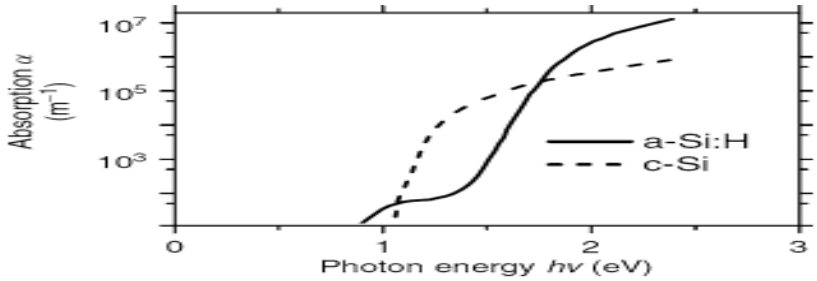

Figure (4) The optical absorption coefficient versus photon energy for (c-Si) and (α-Si:H)(Böer,2013)

2.3.2 Staebler–Wronski Effect

The main phenomenon that reduces the efficiency of amorphous silicon solar cells during the first hours of light exposure is the Staebler–Wronski Effect. Increase the light exposure leads to change in the hydrogen density since the silicon hydrogen bonds are damaged. Hence, the dangling bonds, which are defects, increase gradually, particularly during the first hundred hours of light exposure. As a result of this, the recombination of generated charges (electron-hole) will increase resulting in reducing the solar cell efficiency. Typically, after the first hundred hours of light soaking the cell performance tends to be stable (Radue and Dyk, 2010). Such degradation effect can be recovered by heating the cells to about 150 °C for a few hours (thermal annealing) (Deng et al., 2005).Figure (5) shows the trend of the Staebler–Wronski effect during the illumination

time using a solar simulator (100 mW/cm^2) for a single-junction and for a triple-junction amorphous silicon cells (Deng and Schiff , 2003).

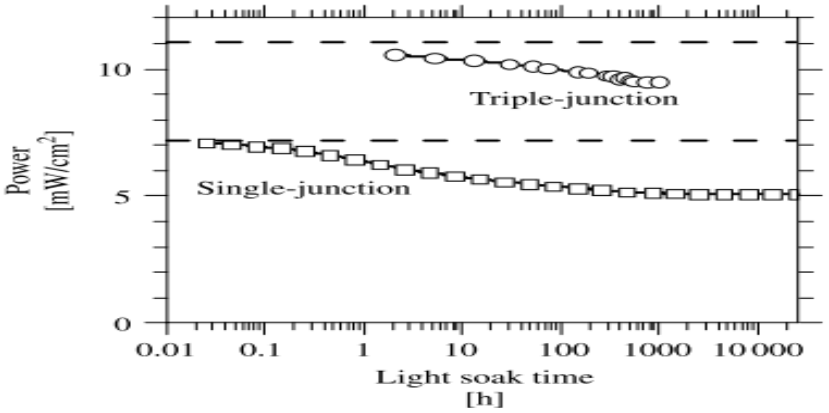

Figure (5) The power output of single-junction and triple-junction (a-si:H) during light exposure (Deng and Schiff, 2003).

3 Methodology

Experiment will be conducted to evaluate the performance (I_{sc}, V_{oc} and hence η) of an amorphous silicon cell over the wavelength range from IR to UV regions. To carry this experiment four equipment should be used:

1-Light source:

A solar simulator (Newport) will be used to supply an approximate spectral that is similar to solar spectra AM 1.5. Experimentally, this provides a simulation of solar irradiance for PV performance measurement. Figure (4) shows the spectral irradiance of the sunlight compared to the wavelength. To enhance the performance of the device, a large range of the solar spectral should be exploited. The graph below presents the standard solar spectra air mass 1.5.

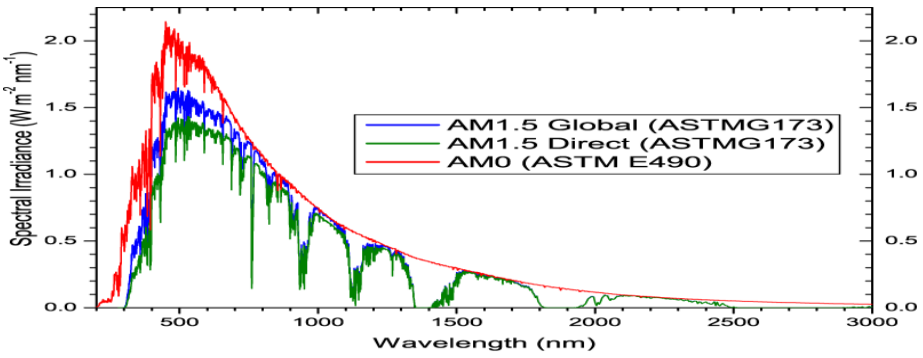

Figure (6) Spectral irradiance versus the wavelength [http://www.pveducation.org]

2- I/V Ammeter:

The HP Picoammeter / DC Voltage Source will be used to provide a voltage supply and to measure the current- voltage characteristic. The measured data will be sent to a connected computer where graphs will be plotted.

3- Materials:

i. A calibrated crystalline silicon cell (NPL) with a known efficiency will be used as a reference cell.

ii. An amorphous silicon cell as the tested cell whose efficiency will be examined.

4- Filters:

Filters will be used to modify the spectral length IR, red and UV.

Firstly, light will be exposed on a calibrated silicon cell and an amorphous silicon cell. A special plate, where the cells are held on, will be connected to a digital I/V ammeter. Then the generated photocurrent and voltage from the cells will be measured by using the digital Picoametter. The generated photocurrent and voltage will be recorded over the energetic spectrum from IR to UV by using a special filter for each spectrum. This ammeter is connected to pc where the generated I-V curve is saved and presented on the screen. The saved data of the generated photocurrent and voltage from the cells will be analysed using Origin programme (data analysis and graphing programme). Figure (5) shows the measurement setup of the experiment. After that, the efficiency will be calculated over the energetic spectrum by using the equation (2) for both cells. The performance comparison between the crystalline silicon cell and the amorphous silicon cell will be presented by plotting two graphs: current verse voltage curve (I-V) and power conversion efficiency (η) with respect to spectral energy (E). It is expected to see that the crystalline silicon cell has higher efficiency value. Then, the reasons behind the lower efficiency of the amorphous silicon cell will be examined whether it is due to recombination, the structure of the cell, the energy gab, series resistance etc.

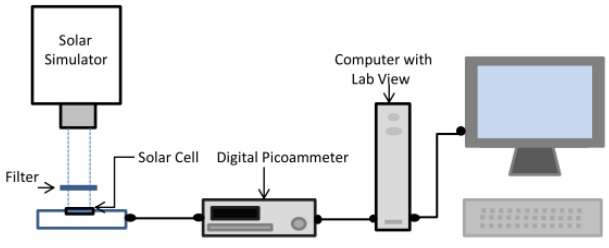

Figure (7) Sketch of the experiment setup.

4 A review of Project Risks

To a low extent, there are some failures that might prevent fulfilling the objectives of the experiment. This could be

- Equipment failure: this random behaviour could happen in all laboratory experiments. Equipment failure rarely exists as the laboratory equipment of the university is frequently tested. This kind of failure increases the risk of meeting the project aim in its time frame. Nothing could be done to mitigate this cause of risk as it is out of control.
- Human error/mistakes during the experiment (practical failure). The probability of the human error is medium. If happens, it will lead to repeat the experiment which causes the risk of completing the project on time. To mitigate this risk, the instruction and the experiment plan should strictly be followed to keep the experiment environment as accurate as previously described.
- Failure in collecting a complete data set, for example, incomplete filtering in time available. This could occur with low probability. As a result, it causes a delay in project time schedule. By following the project time schedule, a complete set of data will be achieved in the time allotted.
- Deviation from project aim and objectives. In consequence, the main aim of the project will not be meet. However, this risk probability is very low as there will be regular meetings with the supervisor when some assists and guidance will be provided.
- IT failure, for example, damage or loss of personal pc where the data saved, and hence, the data will be lost. Consequently, all the experiment procedure will be redone which increase the risk of accomplishing the project before the deadline. In spite of the low probability of happing, a data backup will be saved in different pcs, online drives such as Google drive, drop box, or flash memory.

5 Project planning

This project should be completed and submitted in twelve weeks. Project tasks are planned to be done in an adequate time schedule. Firstly, there will be a time (three weeks) for more research about the indoor efficiency measurement of solar cells and the amorphous silicon cell properties. Three weeks is enough time for a broader understanding and for generating a critical literature review. Fortunately, the experiment itself does not take much time, around three day. The total completion of the measurements, however, has been assigned four weeks in order to count for lab availability, equipment familiarisation, failure risks and repetition of the experiment. Most of the measurement time will be to learn how the equipment is used and how the data is analysed.

The rest time will be allotted for generating the dissertation including writing, revision, proofreading, and finally printing and binding. The Gantt Chart shown below provides detailed time plan of the project.

Activity ID	Activity Title	Duration [Day/s]	Start	Finish	Wk.1	Wk.2	Wk.3	Wk.4	Wk.5	Wk.6	Wk.7	Wk.8	Wk.9	Wk.10	Wk.11	Wk.12	1 Sep
	Research	21	2/6/2014	22/6/2014													
1	Complete the research in more details	21	2/6/2014	22/6/2014													
	Experiments	28	23/6/2014	20/7/2014													
2	Learning the equipment	4	23/6/2014	26/6/2014													
3	Measure the solar cells	10	27/6/2014	6/7/2014													
4	Analysing data	10	7/7/2014	16/7/2014													
5	Draw the graphs	4	17/7/2014	20/7/2014													
	Dissertation writing preparation	42	21/7/2014	1/9/2014													
6	First draft	23	21/7/2014	12/8/2014													
7	Proof reading	4	13/8/2014	16/8/2014													
8	Discuss the report draft with the supervisor	5	17/8/2014	21/8/2014													
9	Revison	6	22/8/2014	27/8/2014													
10	Printing and binding	3	28/8/2014	30/8/2014													
11	Submission	1	1/9/2014	1/9/2014													

6 References

Böer, K.W. (2013) 'Amorphous Silicon Solar Cells': *Handbook of the Physics of Thin-Film Solar Cells*, pp.721-738. DOI 10.1007/978-3-642-36748-9_41, © Springer-Verlag Berlin Heidelberg.

Deng, J., Pearce, J. M., Albert, M. L., Wronski, C. R. and Collins, R.W. (2005) , 'Room Temperature Annealing of Fast States from 1 sun Illumination in Protocrystalline Si:H Materials and Solar Cells', *31st IEEE Photovoltaic Specialists Conf. Proc*., (IEEE, 2005) pp. 1536-1539.

Deng, X. and Schiff, E. (2003) 'Amorphous Silicon–based Solar Cells' in A. Luque and S. Hegedus (eds.) *Handbook of Photovoltaic Science and Engineering*. John Wiley & Sons, Ltd, pp. 505-565. ISBN: 0-471-49196-9.

Editorial (2008) 'Reporting solar cell efficiencies in Solar Energy Materials and Solar Cells', *Solar Energy Materials & Solar Cells*, (92) 371-373.

Emery, K. (2003) 'Measurement and Characterization of Solar Cells and Modules' in A. Luque and S. Hegedus (eds.) *Handbook of Photovoltaic Science and Engineering*. John Wiley & Sons, Ltd, pp. 701-752. ISBN: 0-471-49196-9.

Emery, K. and Osterwald, C. (1989) Sol. Cells (27), pp. 445–453.

Emery, M. and Moriarty, T. (2008) 'Accurate measurement of organic solar cell efficiency', National Renewable Energy Laboratory, 1617 Cole Blvd., Golden, CO 80401, USA.

Emery, K. et al., (1985) Proc. 18th IEEE Photovoltaic Specialist Conf., 623–628.

FÖll, H.,(2011) Characteristics of Real Solar Cell: Semiconductor Technology. Available at: http://www.tf.uni-kiel.de/matwis/amat/semitech_en/index.html (Accessed: 27 April 2014)

Green, M. at el. (2010). Solar cell efficiency tables (version 36). PROGRESS IN PHOTOVOLTAICS: RESEARCH AND APPLICATIONS. 18, 346–352.

Haberlin, N. (2012) Photovoltaics System Design and Practice: Translated By Herbert Eppel: John Wiley & Sons Inc., eISBN-13: 9781119977001 eISBN-10: 1119977002 Print ISBNs: HB: 9781119992851, 1119992850.

Julian Chen, C. (2011) Physics of Solar Energy: John Wiley & Sons Inc., eISBN-13: 9781118044575 eISBN-10: 1118044576 Print ISBNs: HB: 9780470647806, 0470647809.

KEITHELY Instrument Application Note Series (2000) Making I‑V and C‑V Measurements on Solar/Photovoltaic Cells Using the Model 4200‑SCS Semiconductor Characterization System. Available at http://www.keithley.com/data?asset=50913 (Accessed: 4 April 2014).

Nann, S. and Emery, K. (1992) Sol. Energy Mate (27), 189–216.

Radue, C. and Dyk, E.E. (2010) 'A comparison of degradation in three amorphous silicon PV module technologies ', *Solar Energy Materials & Solar Cells*, (94), pp.617–622

Standard Solar Spectra Available at: http://www.pveducation.org/pvcdrom/appendices/standard-solar-spectra (Accessed: 4 July 2014)

Tao, M. (2014) Physics of Solar Cells, In: Terawatt Solar Photovoltaics. London: Springer, pp. 21-45.

The University of Manchester

General Risk Assessment Form

Date: (1)	Assessed by: (2)	Checked / Validated* by: (3)	Location: (4)	Assessment ref no (5)	Review date: (6)
7/5/2014	Nouf Alkathran	Prof. Bruce Hamilton	Alan Turing Building Lab 1.316		3 months
Task / premises: (7)					

Activity (8)	Hazard (9)	Who might be harmed and how (10)	Existing measures to control risk (11)	Risk rating (12)	Result (13)

Activity (8)	Hazard (9)	Who might be harmed and how (10)	Existing measures to control risk (11)	Risk rating (12)	Result (13)
Measurement and observation.	Work Stations:	University staff/student. Back strain (poor posture); Eye strain.	1-Ensure that computer workstations are usually under assessment. Self assessment 'tool' and guidance available on staff intranet. 2. Schedule work to ensure having regular breaks from the computer	Low	T
Researching, Studying, and conducting experiments	Electrical: Computer, printer, desk lamp, fan, heater, photocopier, shredder, extension leads.	University (staff/ students), visitors, and cleaners. Electric shock and or burns	1. Using all office equipment according to the manufacturers instructions. 2. Reporting about defective plugs, cables equipment etc to Laboratories Manager for repair/replacement. 3. Reduce the need for extension cables by providing sufficient power sockets. 4. Do not bring own electrical equipment because their maintenance cannot be assured.	Low	A

Activity (8)	Hazard (9)	Who might be harmed and how (10)	Existing measures to control risk (11)	Risk rating (12)	Result (13)
Researching, Studying, and conducting experiments at the university facilities	Fire: Fire offices or laboratories	University (staff/students), visitors, cleaners. Risk of burns, smoke inhalation, asphyxiation	1. Fire alarms are tested every week. 2. All staff and students are given instruction about the fire evacuation procedures and for raising the alarm 3. Annually, fire evacuation practices are carried out. 4. Fire exits should be kept clear and escape routes clearly identified. 5. Ready access to fire extinguishers in each floor. 6. Fire alarm points in adjacent corridors and stair well landings. 8. Removing combustible waste, regularly. 9. All heaters should be placed away from combustible materials.	Medium	A

Activity (8)	Hazard (9)	Who might be harmed and how (10)	Existing measures to control risk (11)	Risk rating (12)	Result (13)
Manual handling	Crush injuries, strains and sprains, bruising.	University (staff/ students), visitors, cleaners. Moving heavy, large loads.	1. Basic instruction about safe manual handling is given to the university staff and students. 2. For moving large/heavy furniture etc., contact School services. 3. Do not store large/heavy items at high place (e.g. high shelves). 4. Using a trolley to move heavy items.	Low	A
Slips, trips	Crush injuries, strains, sprains, bruising or fractures.	University (staff/ students), visitors, cleaners.	1. Reporting immediately about damage to floor coverings and other repairs to Laboratories Manager for repair/replacement. 2. Keeping floors and ways clear of items, e.g. equipment, boxes etc. 3. Keeping cabinet drawers and doors closed. 4. Cleaned and drying floor regularly. 5. Providing adequate lighting to ensure good sight.	Low	A

Activity (8)	Hazard (9)	Who might be harmed and how (10)	Existing measures to control risk (11)	Risk rating (12)	Result (13)
Pressure of work,	Stress related illness or complaint.	University (staff/ students). Poor aid from colleagues or line management, insufficient knowledge of role or poor working/professional relationships.	1. The University has a stress policy. 2. Discussing projects or work plans frequently. 3. Consulting The Occupational Health Service if it is necessary.	Medium	T
Working Environment: Heating, Ventilation, cooling, lighting and hygiene.	Occupant health, comfort and performance.	University (staff/ students).	1. Providing an adequate heating /cooling. 2. Ensuring good level of ventilation. 3. Providing good level of lighting especially at the top of desks. 4. Providing well maintained toilet facilities in each building.	Low	T

Activity (8)	Hazard (9)	Who might be harmed and how (10)	Existing measures to control risk (11)	Risk rating (12)	Result (13)
Bringing personal equipment such as laptop, I pad, etc.	Stolen	University stuff/students. Leaving such devices without monitoring could increase the risk of theft.	Keeping your devices with you or keep them with a trusted friend.	Low	T

Action plan (14)				
Ref No	**Further action required**	**Action by whom**	**Action by when**	**Done**